Cannabinoid signaling promotes the reprogramming of Muller glia into proliferating progenitor cells.

Abbreviated title: Cannabinoid signaling promotes Müller glia reprogramming

Warren A. Campbell[1], Sydney Blum[1], Alana Reske[1], Thanh Hoang[2], Seth Blackshaw[2], Andy J. Fischer[1]*

1 Department of Neuroscience, College of Medicine, The Ohio State University, Columbus, OH

2 Solomon H. Snyder Department of Neuroscience, Johns Hopkins University School of Medicine, Baltimore, MD

***corresponding author**: Andy J. Fischer, Department of Neuroscience, Ohio State University, College of Medicine, 3020 Graves Hall, 333 W. 10th Ave, Columbus, OH 43210-1239, USA. Telephone: (614) 292-3524; Fax: (614) 688-8742; email: Andrew.Fischer@osumc.edu

Author Contributions: WAC and executed experiments, gathered data, constructed figures, and contributed to writing the manuscript. SB and AR executed experiments, and gathered data. AJF designed experiments, analyzed data, constructed figures, and wrote the manuscript.

Acknowledgements: This work was supported by RO1 EY022030-08, RO1 EY032141-01 (AJF) and UO1 EY027267-04 (AJF).

Word count: 9697

Abstract

Endocannabinoids (eCB) are lipid-based neurotransmitters that are known to influence synaptic function in the visual system. eCBs are also known to suppress neuroinflammation in different pathological states. However, nothing is known about the roles of the eCB system during reprogramming of Müller glia (MG) into proliferating progenitor-like cells in the retina. Accordingly, we used the chick and mouse model to characterize expression patterns of eCB-related genes and applied pharmacological agents to examine how the eCB system impacts glial reactivity and the capacity of MG to become Müller glia-derived progenitor cells (MGPCs). We probed single cell RNA-seq libraries to identify eCB-related genes and identify cells with dynamic patterns of expression in damaged retinas. MG and inner retinal neurons expressed the eCB receptor *CNR1*, as well as enzymes involved in eCB metabolism. In the chick, intraocular injections of 2-Arachidonoylglycerol (2-AG) and Anandamide (AEA) potentiated the formation of MGPCs. Consistent with these findings, CNR1-agonists and MGLL-inhibitor promoted reprogramming, whereas CNR1-antagonist and inhibitors of eCB synthesis suppressed reprogramming. Surprisingly, retinal microglia were largely unaffected by increases or decreases in eCB signaling in both chick and mouse models. However, eCB-signaling suppressed the activation of NFkB-reporter in MG in damaged mouse retinas. We conclude that the eCB system in the retina influences the reactivity of MG and is important for regulating glial reactivity and the reprogramming of

MG into proliferating MGPCs, but not for regulating the reactivity of immune cells in the retina.

Keywords: Endocannabinoids, Müller glia, Müller glia derived progenitor cells, scRNA-seq, Müller glia reprogramming

Main Points

Müller glia express CNR1 receptor and endocannabinoid synthesis genes.

Endocannabinoids after retinal damage promote the formation of Müller glia derived progenitor cells in chick.

Endocannabinoids reduce NFkB activity in mouse Müller glia.

Introduction

The endocannabinoid (eCB) system has been well-studied in the visual system and is known to modulate physiologic functions in different ocular tissues, including the retina (reviewed by (Schwitzer et al., 2016). The eCB system consists of cannabinoid receptors 1 and 2 (*CNR1*, *CNR2*), endogenous ligands 2-Arachidonoylglycerol (2-AG) and Arachidonoylethanolamide (AEA), and the enzymes that control ligand synthesis and degradation. The eCB pathway has been identified in the retinas of different vertebrates including embryonic chick (da Silva Sampaio et al., 2018), goldfish (Yazulla et al., 2000), rat (Yang et al., 2016), bovine (Bisogno et al., 1999), porcine (Matsuda et al., 1997), mouse (Hu et al., 2010), and human (Straiker et al., 1999). The expression of CNR1 and CNR2 receptors in the central nervous system varies across species but typically includes distinct types of neurons, astrocytes, microglia, and Müller glia. Activation of eCB receptors is known to modulate neurotransmission (Diana and

Bregestovski, 2005), synaptic plasticity (Xu and Chen, 2015), neuroinflammation (Centonze et al., 2007), and neuroprotection (Slusar et al., 2013).

Müller glia (MG) are thought to play a role in regulating eCBs in the retina. Both CNR1 and CNR2 receptors have been identified in goldfish MG (Yazulla et al., 2000), and CNR2 receptors have been identified in the retinas of vervet monkeys (Bouskila et al., 2013). eCBs have been shown to modify activity or suppress T-type voltage gated calcium channels in rat MG (Yang et al., 2016) and modulate the inflammatory micro-environment (Silverman and Wong, 2018). MG possess pathogen- and damage-associated molecular pattern (PAMP/DAMP) receptors to respond to pathological conditions (Kumar and Shamsuddin, 2012; Kumar et al., 2013; Shamsuddin and Kumar, 2011). Activation leads to the secretion of pro-inflammatory cytokines to facilitate the migration and activation of macrophages and microglia (Inoue et al., 1996). At the same time, retinal microglia become reactive and coordinate inflammation with MG, which results in NF-kB activation, concomitant reactive gliosis, and formation of MGPCs (Palazzo et al., 2019). However, MG also produce anti-inflammatory signals such as TGFB2 (Palazzo et al., 2020) and TIMP3 (Campbell et al., 2019) to suppress inflammation. eCBs are believed to have anti-inflammatory actions within the central nervous system (Nagarkatti et al., 2009). Little is known about how eCBs influence inflammation in the retina and whether eCBs impact the ability of MG to reprogram into MG-derived progenitor cells (MGPCs).

The impact of inflammatory signals on MG is context specific, dependent on the combination of cytokines and the model of damage. In zebrafish, TNFa (Iribarne et al., 2019) and IL-6 (Zhao et al., 2014) are necessary for MG to transition to a reactive state

into a proliferating progenitor-like cells. In the chick, by comparison, TNF alone does not induce MGPCs and activation of the NF-kB pathway inhibits the formation of MGPCs (Hoang et al., 2020; Palazzo et al., 2020). When microglia are ablated, MGPCs fail to form (Fischer et al., 2014), and the effects of NF-kB-inhibition are reversed to promote the formation of MGPCs (Palazzo et al., 2020). In damaged mouse retinas, reactive MG rapidly transition into a gliotic state and are forced back into a resting state, in part, by regulatory networks involving NF-kB-related factors (Hoang et al., 2020). This suggests that there is an important balance of inflammatory cytokines and timing of signals to drive the reprogramming of MG to dedifferentiate and proliferate as MGPCs. It is currently thought that rapid induction of microglial reactivity is required to "kick-start" MG reactivity as an initial step of reprogramming (Fischer et al., 2014; White et al., 2017), whereas sustained elevated microglial reactivity suppresses the neuronal differentiation of progeny produced by MGPCs (Palazzo et al., 2020; Todd et al., 2020).

In this study we investigate how eCBs influence glial reactivity, inflammation, and reprogramming of MG in the chick retina. Using scRNA-seq, we analyze the expression pattern of genes in the eCB system and changes in these genes following retinal damage. We apply pharmacological agents to activate or inhibit eCB-signaling and assess changes in glial activation and reprogramming of MG into proliferating MGPCs.

Methods and Materials:

Animals:

The animals approved in these experiments followed guidelines established by the National Institutes of Health and IACUC at The Ohio State University. P0 wildtype

leghorn chicks (*Gallus gallus domesticus*) were obtained from Meyer Hatchery (Polk, Ohio). Post-hatch chicks were housed in stainless-steel brooders at 25^{o}C with a diurnal cycle of 12 hours light, 12 hours dark (8:00 AM-8:00 PM) and provided water and Purina^{tm} chick starter *ad libitum*.

Intraocular injections:

Chicks were anesthetized with 2.5% isoflurane mixed with oxygen from a non-rebreathing vaporizer. The intraocular injections were performed as previously described (Fischer et al., 1998). With all injection paradigms, both pharmacological and vehicle treatments were administered to the right and left eye respectively. Compounds were injected in 20 µl sterile saline with 0.05 mg/ml bovine serum albumin added as a carrier. Compounds included: NMDA (500nmol dose high dose, 60nmol low dose; Sigma-Aldrich), JJKK048 (0.25mg/dose Sigma-Aldrich), ARN19874 (0.25mg/dose AOBIOUS), rimonabant (0.25mg/dose Sigma-Aldrich), PF 04457845 (0.25mg/dose Sigma-Aldrich), Orlistat (0.25mg/dose Sigma-Aldrich), URB 597 (0.25mg/dose Sigma-Aldrich). 5-Ethynyl-2´-deoxyuridine (EdU) was intravitreally injected to label the nuclei of proliferating cells. Injection paradigms are included in each figure.

Enzyme-linked Immunosorbent Assay

Endocannabinoids were extracted from retinal tissue and screened for 2-AG levels using a direct competitive enzyme linked immunosorbent assay (MyBioSource). Three retinas were extracted from each treatment group and placed in 5:3 homogenization solution (formic acid pH = 3): extraction solution (9:1

ethylacetate:hexane) on ice. The tissue was homogenized with high intensity sonication on ice, frozen at -20, and the nonaqueous fraction was removed for evaporation and rehydration in DMSO. The lipid extract was applied to the wells of ELISA and the protocol was followed per the manufacturer's instructions.

Single Cell RNA sequencing of retinas

Retinas were obtained from postnatal chick and adult mice. Isolated retinas were dissociated in a 0.25% papain solution in Hank's balanced salt solution (HBSS), pH = 7.4, for 30 minutes, and suspensions were frequently triturated. The dissociated cells were passed through a sterile 70µm filter to remove large particulate debris. Dissociated cells were assessed for viability (Countess II; Invitrogen) and cell-density diluted to 700 cell/µl. Each single cell cDNA library was prepared for a target of 10,000 cells per sample. The cell suspension and Chromium Single Cell 3' V3 reagents (10X Genomics) were loaded onto chips to capture individual cells with individual gel beads in emulsion (GEMs) using 10X Chromium Controller. cDNA and library amplification for an optimal signal was 12 and 10 cycles respectively. Samples were multiplexed for sequencing on Illumina's Novaseq6000 (Novogene). Sequencer files were converted from a BCL to a Fastq format, where the sequence files were de-multiplexed, aligned, and annotated using the chick ENSMBL database (GRCg6a, Ensembl release 94) and Cell Ranger software (10x Genomics). Using Seurat toolkits, Uniform Manifold Approximation and Projection for Dimension Reduction (UMAP) plots were generated from aggregates of multiple scRNA-seq libraries (Butler et al., 2018; Satija et al., 2015). Compiled in each UMAP plot are two biological library replicates for each experimental condition. Seurat

was used to construct violin/scatter plots. Significance of difference in violin/scatter plots was determined using a Wilcoxon Rank Sum test with Bonferroni correction. Genes that were used to identify different types of retinal cells included the following: (1) Müller glia: *GLUL, VIM, SCL1A3, RLBP1*, (2) MGPCs: *PCNA, CDK1, TOP2A, ASCL1*, (3) microglia: *C1QA, C1QB, CCL4, CSF1R, TMEM22*, (4) ganglion cells: *THY1, POU4F2, RBPMS2, NEFL, NEFM*, (5) amacrine cells: *GAD67, CALB2, TFAP2A*, (6) horizontal cells: *PROX1, CALB2, NTRK1*, (7) bipolar cells: *VSX1, OTX2, GRIK1, GABRA1*, and (7) cone photoreceptors: *CALB1, GNAT2, OPN1LW*, and (8) rod photoreceptors: *RHO, NR2E3, ARR3.* scRNA-seq libraries can be queried at:

https://proteinpaint.stjude.org/F/2019.retina.scRNA.html

Fixation, sectioning, and immunocytochemistry:

Ocular tissues were fixed, sectioned, and labeled via immunohistochemistry as described previously (Fischer et al., 2008, 2009a). Dilutions and commercial sources of antibodies used in this study are listed in table 2. Labeling was not due to non-specific labeling of secondary antibodies or tissue autofluorescence because sections incubated with secondary antibodies alone were devoid of fluorescence. Secondary antibodies included donkey-anti-goat-Alexa488/568, goat-anti-rabbit-Alexa488/568/647, goat-anti-mouse-Alexa488/568/647, goat-anti-rat-Alexa488 (Life Technologies) diluted to 1:1000 in PBS and 0.2% Triton X-100.

Labeling for EdU:

For the detection of nuclei that incorporated EdU, immunolabeled sections were fixed in 4% formaldehyde in 0.1M PBS pH 7.4 for 5 minutes at room temperature.

Samples were washed for 5 minutes with PBS, permeabilized with 0.5% Triton X-100 in PBS for 1 minute at room temperature and washed twice for 5 minutes in PBS. Sections were incubated for 30 minutes at room temperature in a buffer consisting of 100 mM Tris, 8 mM $CuSO_4$, and 100 mM ascorbic acid in dH_2O. The Alexa Fluor 568 Azide (Thermo Fisher Scientific) was added to the buffer at a 1:100 dilution.

Terminal deoxynucleotidyl transferase dUTP nick end labeling (TUNEL):

The TUNEL assay was implemented to identify dying cells by imaging fluorescent labeling of double stranded DNA breaks in nuclei. The *In Situ* Cell Death Kit (TMR red; Roche Applied Science) was applied to fixed retinal sections as per the manufacturer's instructions.

Photography, measurements, cell counts and statistics:

Microscopy images of retinal sections were captured with the Leica DM5000B microscope with epifluorescence and the Leica DC500 digital camera. High resolution confocal images were obtained with a Leica SP8 available in The Department of Neuroscience Imaging Facility at The Ohio State University. Representative images are modified to have enhanced color, brightness, and contrast for improved clarity using Adobe Photoshop. In EdU proliferation assays, a fixed region of retina was counted and average numbers of Sox2 and EdU co-labeled cells. The retinal region selected for investigation was standardized between treatment and control groups to reduce variability and improve reproducibility.

Similar to previous reports (Fischer et al., 2009b, 2009c; Ghai et al., 2009), immunofluorescence was quantified by using Image J (NIH). Identical illumination, microscope, and camera settings were used to obtain images for quantification. Retinal areas were sampled from 5.4 MP digital images. These areas were randomly sampled over the inner nuclear layer (INL) where the nuclei of the bipolar and amacrine neurons were observed. Measurements of immunofluorescence were performed using ImagePro 6.2 as described previously (Ghai et al., 2009; Stanke et al., 2010; Todd and Fischer, 2015). The density sum was calculated as the total of pixel values for all pixels within thresholded regions. The mean density sum was calculated for the pixels within threshold regions from ≥5 retinas for each experimental condition. GraphPad Prism 6 was used for statistical analyses.

Measurements of immunofluorescence of CD45 in microglia were made from single optical confocal sections by selecting the total area of pixel values above threshold (≥70) for CD45 immunofluorescence. Measurements were made for regions containing pixels with intensity values of 70 or greater (0 = black and 255 = saturated). The total area was calculated for regions with pixel intensities above threshold. The intensity sum was calculated as the total of pixel values for all pixels within threshold regions. The mean intensity sum was calculated for the pixels within threshold regions from ≥5 retinas for each experimental condition. For characterization of the morphology of the individual microglia, a Sholl analysis was used to characterize the size, sphericity, and projections (ImageJ).

For statistical evaluation of differences across treatments, a two-tailed paired *t*-test was applied for intra-individual variability where each biological sample also served

as its own control. For two treatment groups comparing inter-individual variability, a two-tailed unpaired *t*-test was applied. For multivariate analysis, an ANOVA with the associated Tukey Test was used to evaluate any significant differences between multiple groups.

Results:

Patterns of expression of eCB-related genes

scRNA-seq libraries were aggregated from control retinas and retinas treated with NMDA-damage at different times (3, 12 and 48 hrs) after treatment. These libraries were clustered and analyzed for expression eCB-related genes under MG-reprogramming conditions (Fig. 1). UMAP plots were generated and the identity of clusters of cells established based on expression of cell-distinguishing markers (Fig. 1b,c). Resting MG occupied a discrete cluster of cells and expressed high levels of *GLUL, VIM* (Fig. 1d)*, RLBP1* and *CA2* (supplemental Fig. 1a-e,i). After damage, MG down-regulate these genes during transition to a reactive phenotype and up-regulate markers associated reactivity such as *MDK, HBEGF, MANF* (Fig. 1e, supplemental Fig. 1e,f,i), with some genes such as *TGFB2, ATF3* and *TNFRSF1A* upregulated with 3hrs of NMDA-treatment (supplemental Fig. 1f,g,i). Upregulation of progenitor- and proliferation-related genes was observed in MGPCs at 48hrs after NMDA-treatment

(supplemental Fig. 1c,h,i), consistent with prior reports (Hoang et al., 2020; Campbell et al., 2021,).

The expression of eCB-related genes in MG has been previously reported in developing chick retina (da Silva Sampaio et al., 2018). The eCB system includes receptors *CNR1* and *CNR2* and enzymes involved in the synthesis (*NAPEPLD, DAGLA* and *DAGLB*) and degradation (*FAAH* and *MGLL*) of 2-AG and AEA (Fig. 1a). We detected *CNR1*, *MGLL*, *DAGLA, DAGLB, NAPELPD and FAAH* in control retinas and at different times after NMDA-treatment (Fig. 1f-i). *CNR2* was not detected. *MGLL* was prevalent and highly expressed by resting MG, but down-regulated in activated MG (Fig. 1g,f). By comparison, levels of expression and prevalence of *CNR1* was high in many amacrine cells, and in a few ganglion and bipolar cells (Fig. 1f). *MGLL* and *NAPEPLD* were detected at high levels in many microglia, NIRG cells and bipolar cells, and in relatively few photoreceptors, ganglion and horizontal cells (Fig. 1e). *DAGLA* and *FAAH* had scattered expression across many retinal cell types, whereas *DAGLB* was prominently expressed at high levels in photoreceptors and inner retinal neurons (Fig. 1h). *CNR1* and eCB-related genes, except *FAAH*, were uniformly down-regulated in levels, but increased in prevalence in activated MG after NMDA-treatment (Fig. 1g-i).

To directly compare expression levels in MG across different treatment paradigms we isolated and re-aggregated MG from different treatment groups, including retinas treated with the combination of NMDA+insulin+FGF2, NMDA alone and insulin+FGF2 alone. Resting MG, activated MG from 24 hrs after NMDA-treatment and 2 doses of insulin+FGF2 formed distinct clusters of cells (Fig. 2a,b). Further, MGPCs formed discrete regions of cells wherein cell cycle progression formed the basis of

spatial segregation with the majority of cells progressing through the cell cycle from retinas at 72 hrs after NMDA or NMDA+FGF2+insulin treatment (Fig. 2c,e). The largest increase in levels and prevalence of expression of *CNR1* was observed in reactive MG from 48+72hrs after NMDA (Fig. 2f,g). By comparison, the largest decrease in levels and prevalence of expression of *MGLL, DAGLA, DAGLB* and *NAPEPLD* were observed for MG clustered among treatments with insulin+FGF2 and in the MGPC3 cluster (Fig. 2f,g). Collectively, these findings suggest that the expression of *CNR1* by MG is changed in response to neuronal damage, whereas levels of *MGLL* and other eCB-related genes were down-regulated by treatment with NMDA (neuronal damage) or insulin and FGF2 (no neuronal damage).

eCBs promote the formation of MGPCs after damage

Although patterns of gene expression can be complex and context dependent, dynamic changes in mRNA levels are strongly correlated with changes in protein levels and function (Liu et al., 2016). Accordingly, we tested activation of eCB-signaling influence glial reactivity, neuronal survival and the formation of MGPCs. The ligand binding affinity of chick CNR receptors remains uncertain. Thus, 2-AG and AEA were co-injected to maximize the probability of activation of CNR1 receptors. We tested whether co-injection of 2-AG and AEA influenced the formation of proliferating MGPCs. Compared to numbers of proliferating MGPCs in NMDA-damaged retinas, treatment with eCBs resulted in a significant increase in numbers of Sox2/EdU-positive MGPCs (Fig. 3a,b). Consistent with these findings, numbers of proliferating MGPCs that expressed neurofilament and phospho-histone H3 (pHH3) were significantly increased

by treatment with 2-AG and AEA (Fig. 3c,d). Levels of retinal damage influence the reprogramming of MG; there is a positive correlation between numbers of dying cells and numbers of proliferating MGPCs (Fischer and Reh, 2001; Fischer et al., 2004). Accordingly, we probed for numbers of dying cells by labeling for fragmented DNA using the TUNEL method. The number of TUNEL-positive cells was unchanged by 2-AG and AEA, suggesting that levels of cell death in NMDA-damaged retinas were unaffected by addition of eCBs (Fig 3e,f).

Targeting the eCB synthesis and degradation influences MG reprogramming

Since expression levels of eCB-related genes were changed in NMDA-damaged retinas, we investigated whether levels of eCBs were influenced by damage or drugs that interfere with synthesis or degradation of AEA and 2-AG. We applied Orlistat, an inhibitor of DAGL, to reduce eCB synthesis and JJKK-048, an inhibitor to MGLL, to suppress eCB degradation (Hillard, 2015). By using competitive inhibition ELISAs, we measured levels 2-AG and AEA in retinas treated with NMDA and inhibitors. We detected low levels of 2-AG in the retina, that did not significantly change with NMDA damage at 72 hours (Fig. 4a). Although we failed to detect a significant change in 2-AG with Orlistat treatment, injections of JJKK-048 resulted in a significant increase in retinal levels of 2-AG (Fig. 4a). AEA was not detectable within the threshold range of the ELISA; thus, inhibitor treatments had no detectable impact on levels of AEA (Fig. 4b). Since levels of AEA fell below levels of detection we did not probe for changes in AEA-levels following treatment with inhibitors of NAPEPLD or FAAH.

We next tested whether inhibition of enzymes that produce or degrade eCBs influence glial reactivity, cell death and the formation of MGPCs. We also targeted the

CNR1 receptor with a small molecule agonist and an antagonist. Win-55, 212-2 (Win55) is a potent CNR agonist in humans, mice and chickens (Stincic and Hyson, 2011). Rimonabant is a potent and selective antagonist that inhibits CNR1-mediated cell-signaling (Ádám et al., 2008) (Hillard, 2015). Activation of CNR1 with Win55 increased numbers of proliferating MGPCs, whereas inhibition of CNR1 with rimonabant had the opposite effect (Fig. 4c,d,e). MGLL inhibitor (JJKK048), which increased levels of 2-AG (Fig. 4a), increased numbers of proliferating of MGPCs (Fig. 4f). By comparison, the DAGL inhibitor Orlistat significantly decreased numbers of MGPCs (Fig 4g). Overall, treatments expected to increase eCB-signaling increased MG reprogramming and treatments to decrease eCB-signaling decreased MG reprogramming.

We next targeted enzymes that influence the synthesis (NAPEPLD) or degradation (FAAH) of AEA. Inhibition of NAPELPD with ARN19784 had no effect upon numbers of proliferating MGPCs (Fig. 5a,b), whereas numbers of proliferating microglia were increased (Fig 5c,d) and numbers of proliferating NIRG cells and dying cells were decreased (Fig. 5e-h). By comparison, inhibition of FAAH with URB597 or PF-044 had no significant effect upon proliferating MGPCs, microglia and NIRG cells, or cell death (Fig. 5d,f,h). We bioinformatically isolated scRNA-seq data for microglia and performed a fine-grain analysis. Microglia formed discrete UMAP clustering of resting and activated microglia from control retinas and retinas at 3, 12 and 48 hrs after NMDA-treatment (Fig. 5i-l). We detected scattered expression of relatively high levels of *MGLL* and *NAPEPLD*, but no expression of *CNR1* (Fig. 5m) or *FAAH* (not shown).

353 Collectively, these data suggests that cells in chick retina support production of
354 2-AG over AEA in the context of damage and reprogramming. Further the reactivity of
355 some microglia and NIRG cells, but not MG, is influenced by inhibition of NAPEPLD,
356 and these responses are consistent with patterns of expression seen in scRNA-seq
357 databases.
358
359 **Microglia Reactivity and eCBs**
360 Retinal microglia serve homeostatic functions and mediate inflammation in
361 response to damage and pathogens (Silverman and Wong, 2018). In response to
362 excitotoxic damage in the chick, the microglia become reactive, leading to accumulation
363 of monocytes, proliferation, and upregulation of inflammatory cytokines (Fischer et al.,
364 2014). Given the known association of microglia, inflammation and eCB-signaling
365 (Stella, 2009) and the dependence of MGPC formation on signals provided by reactive
366 microglial (Fischer et al., 2014; Palazzo et al., 2020), we investigated the impact of
367 drugs targeting CNR1 and 2-AG metabolism on microglia reactivity, proliferation and
368 reactivity.
369 Microglia are sparsely distributed and highly ramified when quiescent, but
370 become reactive and transiently accumulate after NMDA-treatment (Fischer et al.,
371 2014). We applied established metrics of microglia reactivity in the chick model (Gallina,
372 2015), including microglia infiltration/accumulation, proliferation, CD45-intensity, cell
373 area, and ramification were compared in different eCB targeted treatments. eCBs and
374 small molecule inhibitors had no significant effect on the reactivity of microglia in
375 damaged retinas (Fig. 6). Both the small molecule drugs and 2-AG/AEA did not

influence total numbers of $CD45^+$ cells compared to damage alone (Fig. 6a-c). Similarly, the number of proliferating $CD45^+$ cells was unaffected by eCB treatments in damaged retinas (Fig. 5a-c). Similarly, the area and intensity of $CD45^+$ immunolabeling were unaffected by drugs targeting eCBs (Fig. 6c). Using a Sholl analysis to quantify microglia shape, we quantified the maximum intersections (ramification index), mean intersections (centroid value), and maximum intersection radius (processes distribution). Although the morphology of resting microglia in saline treated retinas was significantly different from the morphology of microglia in NMDA-damaged retinas (Fig. 6d), the morphology of reactive microglia was unchanged by drugs targeting eCB receptors or metabolic enzymes (table 1).

NF-kB activation is reduced in mouse MG when promoting eCB signaling

NF-kB is a transcription factor known to be a primary transductor of the innate and adaptive immunity, and a central mediator of inflammatory responses to pathogens or tissue damage (Liu et al., 2017). In the chick, activation or inhibition of the NF-kB pathway has a significant impact on the ability of MG to become proliferating MGPCs (Palazzo et al., 2020). In the mouse retina, NF-kB-signaling has been implicated a signaling “hub” that may act to drive MG into a reactive state and then back into a resting state (Hoang et al., 2020). Accordingly, we investigated the anti-inflammatory properties of eCBs using the NF-kB reporter in the mouse retina. We used the mouse model because there are no cell-level read-outs of NF-kB-signaling available in the chick (Palazzo et al., 2020).

We first assessed the patterns of expression of eCB-related factors in normal and NMDA-damaged mouse retinas in aggregated scRNA-seq libraries. UMAP analysis of cells from control and damaged retinas revealed discrete clusters of cell types (Fig. 7a). Neurons from control and damaged retinas were clustered together regardless of time after NMDA-treatment (Fig. 7a). By contrast, resting MG, including MG from 48 to 72 hr after NMDA, and activated MG from 3, 6, 12, and 24 hr after treatment were spatially separated across the UMAP plot (Fig. 7c). Consistent with previous reports (Bouchard et al., 2015), *Cnr1* was detected in amacrine and ganglion cells (Fig. 7d), whereas *Cnr2* was not detected at significant levels in any retinal cells (not shown). By comparison, *Daglb* was detected in many retinal neurons including photoreceptors and bipolar cells, and *Mgll* was detected prominently in ganglion cells, glycinergic amacrine cells, and resting MG (Fig. 7e), similar to patterns seen in chick retinas (Fig. 1). *Dagla* was not detected (not shown). Although *Napepld* was not widely expressed, *Faah* had scattered expression in bipolar cells, and rod and cone photoreceptors (Fig. 7f).

We utilized the cis-NF-kB^{eGFP} reporter mouse line to visualize cells where p65 is driving transcription as a read-out of NF-kB-signaling (Magness et al., 2004). In undamaged retinas, NFkB reporter was observed in a few endothelial cell whereas eGFP reporter was not detected in any retinal neurons or glia (Fig. 8a). At 48hrs after NMDA damage significant numbers of MG express NFkB-eGFP (Fig. 8a,b). Treatment with CNR1 agonist Win55 or eCBs (2-AG/AEA) resulted in a significant reduction in numbers of MG that were eGFP-positive (Fig. 8a,c). By contrast, treatment with CNR1 antagonist (Rimonabant) significantly increased numbes of eGFP-positive MG (Fig. 8a,c). To determine if changes in cell death were influenced eCBs we performed

TUNEL staining. There was no change in cell death in retinas treated with eCBs, Rimonabant or Win55 (Fig. 8d,e). In addition, there was there was no obvious change in microglial morphology (Fig. 8f) and no significant change in the accumulation of microglia in damaged retinas treated with eCBs, Rimonabant or Win55 (Fig. 8g). These data suggest that eCBs influence NF-kB signaling in mammalian MG, whereas neuroprotection and microglial reactivity are unaffected.

Discussion:

In this study we investigated the roles of eCB-signaling in the chick model of MG reprogramming. Retinal cells widely expressed both *CNR1* and genes involved in the synthesis and degradation of eCBs. The levels of expression and proportion of MG that express these genes significantly change following damage and during the transition to a proliferating progenitor-like cell. These changes in expression imply functions for eCBs in damaged retinas and during the formation of MGPCs. Indeed, we found that reprogramming of MG into proliferating MGPCs was promoted by eCBs and by CNR1 agonists or enzyme inhibitor that increase retinal levels of 2-AG. Microglia maintained a reactive phenotype in damaged retinas regardless of treatment with eCB drugs. These findings support recent reports that the inflammatory state of MG is important to the transition from resting to reactive, and then to a progenitor-like cell (Fischer et al., 2014; Hoang et al., 2020; White et al., 2017).

eCB signaling gene expression

In the embryonic chick retina the expression of CNR1 and MGLL has been reported in MG (da Silva Sampaio et al., 2018). In addition to expression in MG, we detected *CNR1* in MG and in a population of amacrine cells and MGLL was detected in MG, some types of ganglion cells and oligodendrocytes. The eCB-related genes were present in MG but at low levels in a small proportion of MG. This pattern of expression is in contrast with high-expressing glial markers, such as glutamine synthetase (*GLUL*), retinaldehyde binding protein 1 (*RLBP1*) and carbonic anhydrase 2 (*CA2*) that are detected in >96% of MG in scRNA-seq preparations (Campbell et al., 2021; Palazzo et al., 2020). We believe this may be due to sensitivity limitations of the reagents wherein low-copy transcripts may not be readily detected. It is also possible that a sub-population of MG express eCB-related genes, suggesting heterogeneity among MG types. However, the eCB-expressing MG subsets are scattered homogenously in these clusters and do not correlate with unique markers corresponding to biologically unique subclusters.

Elevated eCBs promote MG reprogramming

Although the roles of eCBs have been investigated in the visual system, little is known about how eCBs influence MG reprogramming in different models of retinal regeneration. We observed that exogenous eCB increased the proportion of MG that formed proliferating MGPCs. This effect was reproduced by inhibition of MGLL with JJKK048 which is expected to increase retinal levels of 2-AG. Similarly, this drug has been validated to target MGLL and increase levels of 2-AG levels in mice (Hillard, 2015). Orlistat has been shown to inhibit DAGL and suppress 2-AG synthesis in

466 humans (Bisogno et al., 2006). Although we observed a decrease in number of
467 proliferating MGPCs with Orlistat treatment, we did not observe a significant decrease in
468 2-AG as measured by ELISA. This may have resulted from the low sensitivity threshold
469 for detecting 2-AG. These lipids represent a very small fraction of total lipids from
470 whole-retina extracts. Alternatively, Orlistat could be targeting fatty acid synthase
471 (FASN), disrupting lipid metabolism to influence retinal levels of 2-AG (Kridel et al.,
472 2004).

473 We examined whether CNR1 may have mediated eCB effects applying selective
474 agonists and antagonists, drugs with validated specificity in the chick CNS (Ádám et al.,
475 2008; Stincic and Hyson, 2011). We observed complimentary effects with Win55 (CNR1
476 agonist) increasing and rimonabant (CNR1 antagonist) decreasing numbers of
477 proliferating MGPCs. Nevertheless, we cannot exclude the possibility that these effects
478 are due to indirect actions at MG given that amacrine and ganglion cells express
479 significant levels of *CNR1* and may have mediated effects on MGPCs through
480 secondary factors. We failed to detect *CNR1* expression among microglia, NIRG cells or
481 oligodendrocytes in normal retinas or after NMDA-treatment.

482 Our findings support the hypothesis that MG are receptive and responsive to
483 eCBs. In different animal models and cell types changes in cell physiology are mediated
484 via interactions and cross-talk with other cell-signaling pathways, such as Notch1
485 (Frampton et al., 2010), mTor (Palazuelos et al., 2012), MAPK/PI-3K (Dalton et al.,
486 2009), and Wnt signaling (Nalli et al., 2019). These cell-signaling pathways are known
487 to be active and promote the reprogramming of MG into MGPCs in the chick model
488 (Fischer et al., 2002; Gallina et al., 2016; Ghai et al., 2010; Zelinka et al., 2016).

However, we have yet to identify the interactions between eCB-signaling and other cell-signaling pathways that have been implicated in the reprogramming of MG. These connections may be difficult to identify in undamaged retinas given that homeostatic enzymes reduce eCB levels and because the sensitivity of MG to eCBs may increase after damage with increased prevalence of *CNR1*-expression among MG.

eCBs are not neuroprotective to excitotoxic NMDA damage

eCBs have been shown to provide neuroprotection in degenerative retinal diseases (Rapino et al., 2018). Recent articles have even suggested that 2-AG can mediate neuroprotection against AMPA toxicity in the rat retina (Kokona et al., 2021). We investigated eCB-related neuroprotection because levels of retinal damage and cell death are known to influence the reprogramming of MG in to MGPCs. Although, injections of 2-AG and AEA did not impact numbers of dying cells, the CNR1 agonist Win55 increased cell death in the chick retina (supplemental Fig. 2a,b). This could result from interactions with ion channels that are known to occur with these lipophilic eCB ligands (Pertwee, 2010). Alternatively, differences in excitotoxicity with eCB administration could be due to targeting NMDA vs AMPA receptors in the damage model. (2021) reported the death of photoreceptors with AMPA-selective agonists, which does not occur with NMDA. In other disease models where 2-AG provides neuroprotection the mode of cellular damage is slow and progressive (Centonze et al., 2007), unlike our model of NMDA-induced excitotoxicity which acute and severe.

Microglia reactivity is not influenced by eCBs

eCBs are believed to be potent anti-inflammatory drugs in the CNS (Ullrich et al., 2007). This is frequently suggested as mechanism of clinical benefit in pathological states. In the chick model of reprogramming, we have used dexamethasone GCR receptor agonist to repress the reactivity of microglia (Gallina, 2015). Similarly, treating damaged retinas with NF-kB inhibitor sulfasalazine also resulted in a decrease in the reactive proliferation of $CD45^+$ cells (Palazzo et al., 2020). With eCBs and small molecule drugs, there was no evidence that the reactivity of the microglia was influenced. Studies have demonstrated that reduced accumulation of reactive microglia results in neuroprotective effects whereas increased accumulation of microglial reactivity can be detrimental to neuronal survival (Fischer et al., 2015; Todd et al., 2019) (Fischer et al., 2105 Glia; Todd et al., 2019 J Neuroinflam; other refs). In the current study, however, inhibition of NAPEPLD increased the accumulation of reactive microglia, while numbers of dying cells were reduced. This may have resulted from multiple cellular targets being directly affected by the NAPEPLD inhibitor since *NAPEPLD* was detected in microglia, MG and inner retinal neurons.

Our findings are consistent with the notion that eCB-signaling is, in part, manifested through MG. However, we cannot exclude the possibility of eCBs mediate changes in production pro-inflammatory cytokines from reactive microglia in damaged retinas. The relationship between these inflammatory factors and MGPC formation is complex and time-dependent. For example, decreased retinal inflammation from inhibition of microglial reactivity with glucocorticoid agonists reduced MGPC formation, whereas decreased retinal inflammation from inhibition of NFkB-signaling increased MGPC formation (Gallina, 2015; Palazzo et al., 2020). However, the impact of NFkB-

signaling on the formation of MGPCs was reversed when the microglia were ablated (Palazzo et al., 2020). Pro-inflammatory factors likely directly influence MG, with evidence that MG activate NF-kB-signaling and express cytokine receptors in damaged retinas (Palazzo et al., 2020). Further studies are required to determine the impact of pro-inflammatory signals on microglia and MG in eCB-treated retinas to better characterize the coordination between these glial cells.

eCBs repress NF-kB in mouse MG

While reporter lines for MG do not exist in the chick model, the mouse model of retinal damage was applied to the cis-NF-kB^{eGFP} reporter line to identify cells where p65 translocates into the nucleus and drives the expression of the eGFP-reporter. We find that MG are the primary cell type that activates NF-kB-signaling in NMDA-damaged retinas. This supports prior findings in chick that MG respond to proinflammatory cytokines such as TNF associated with NF-kB signaling (Palazzo et al., 2020). After damage eCBs reduced numbers of GFP^{+} MG, suggesting that eCBs limit the activation of NF-kB in support cells. NF-kB has been implicated as an important pathway in mouse retina that may mediate a switch between reactive gliosis and resting MG (Hoang et al., 2020). Recent studies focused on MG reprogramming have highlighted the importance of the interactions between microglia and MG. The ablation of microglia with CSF1R inhibitor have a dramatic impact on the neurogenic capacity of MG that overexpress Ascl1 (Todd et al., 2020). The absence of microglia induced transcriptomic changes in MG which included the repression of gliosis-associated genes (Todd et al., 2020). The

context, timing and specific cell-signaling pathways that influence the reprogramming capacity of MG in the mammalian retina requires further investigation.

Conclusions:

In this study we investigated the impact of eCBs on retinal inflammation and MG reprogramming in the chick model. We found transcriptomic evidence of eCB genes expressed by MG and the expression of these genes was dynamic following injury and during the transition into MGPCs. Increasing levels of eCBs through intravitreal injections or upregulation of 2-AG via enzyme inhibitors increased numbers of proliferating MGPCs. Surprisingly, cell death and microglia reactivity were largely unaffected by experimental manipulation of levels eCBs in both chick and mouse models of retinal damage. These data support recent evidence that inflammatory signaling play a pivotal role in regulating reactive gliosis, promoting the de-differentiation in MG, and suppressing the neurogenic capacity of MGPCs.

Author contributions: WAC – experimental design, execution of experiments, collection of data, data analysis, construction of figures and writing the manuscript. SB and AR - execution of experiments, collection of data and data analysis. TH and SB facilitated the single cell experiments. AJF – experimental design, data analysis, construction of figures and writing the manuscript.

Competing Interests: The authors have no competing interests to declare.

580 **Data availability**: RNA-Seq data are deposited in GitHub

581 https://github.com/jiewwwang/Single-cell-retinal-regeneration

582 https://github.com/fischerlab3140/scRNAseq_libraries

583 scRNA-Seq data can be queried at

584 https://proteinpaint.stjude.org/F/2019.retina.scRNA.html.

585

586

587 **References:**

588 Ádám, Á.S., Wenger, T., and Csillag, A. (2008). The cannabinoid CB1 receptor antagonist
589 rimonabant dose-dependently inhibits memory recall in the passive avoidance task in domestic
590 chicks (Gallus domesticus). Brain Research Bulletin *76*, 272–274.

591 Bisogno, T., Delton-Vandenbroucke, I., Milone, A., Lagarde, M., and Di Marzo, V. (1999).
592 Biosynthesis and Inactivation of N-Arachidonoylethanolamine (Anandamide) and N-
593 Docosahexaenoylethanolamine in Bovine Retina. Archives of Biochemistry and Biophysics *370*,
594 300–307.

595 Bisogno, T., Cascio, M.G., Saha, B., Mahadevan, A., Urbani, P., Minassi, A., Appendino, G.,
596 Saturnino, C., Martin, B., Razdan, R., et al. (2006). Development of the first potent and specific
597 inhibitors of endocannabinoid biosynthesis. Biochimica et Biophysica Acta (BBA) - Molecular
598 and Cell Biology of Lipids *1761*, 205–212.

599 Bouchard, J.-F., Casanova, C., Cécyre, B., and Redmond, W.J. (2015). Expression and
600 Function of the Endocannabinoid System in the Retina and the Visual Brain (Hindawi).

601 Bouskila, J., Javadi, P., Casanova, C., Ptito, M., and Bouchard, J.-F. (2013). Müller cells
602 express the cannabinoid CB2 receptor in the vervet monkey retina. Journal of Comparative
603 Neurology *521*, 2399–2415.

604 Butler, A., Hoffman, P., Smibert, P., Papalexi, E., and Satija, R. (2018). Integrating single-cell
605 transcriptomic data across different conditions, technologies, and species. Nature Biotechnology
606 *36*, 411–420.

607 Campbell, W.A., Deshmukh, A., Blum, S., Todd, L., Mendonca, N., Weist, J., Zent, J., Hoang,
608 T.V., Blackshaw, S., Leight, J., et al. (2019). Matrix-metalloproteinase expression and
609 gelatinase activity in the avian retina and their influence on Müller glia proliferation.
610 Experimental Neurology *320*, 112984.

611 Campbell, W.A., Fritsch-Kelleher, A., Palazzo, I., Hoang, T., Blackshaw, S., and Fischer, A.J.
612 (2021). Midkine is neuroprotective and influences glial reactivity and the formation of Müller glia-
613 derived progenitor cells in chick and mouse retinas. Glia *n/a*, 1–25.

614 Centonze, D., Finazzi-Agrò, A., Bernardi, G., and Maccarrone, M. (2007). The endocannabinoid
615 system in targeting inflammatory neurodegenerative diseases. Trends in Pharmacological
616 Sciences *28*, 180–187.

617 Dalton, G.D., Bass, C.E., Van Horn, C., and Howlett, A.C. (2009). Signal Transduction via
618 Cannabinoid Receptors. CNS Neurol Disord Drug Targets *8*, 422–431.

619 Diana, M.A., and Bregestovski, P. (2005). Calcium and endocannabinoids in the modulation of
620 inhibitory synaptic transmission. Cell Calcium *37*, 497–505.

621 Fischer, A.J., and Reh, T.A. (2001). Muller glia are a potential source of neural regeneration in
622 the postnatal chicken retina. Nat Neurosci *4*, 247–252.

623 Fischer, A.J., Seltner, R.L.P., Poon, J., and Stell, W.K. (1998). Immunocytochemical
624 characterization of quisqualic acid- and N-methyl-D-aspartate-induced excitotoxicity in the retina
625 of chicks. Journal of Comparative Neurology *393*, 1–15.

626 Fischer, A.J., McGuire, C.R., Dierks, B.D., and Reh, T.A. (2002). Insulin and Fibroblast Growth
627 Factor 2 Activate a Neurogenic Program in Müller Glia of the Chicken Retina. J. Neurosci. *22*,
628 9387–9398.

629 Fischer, A.J., Schmidt, M., Omar, G., and Reh, T.A. (2004). BMP4 and CNTF are
630 neuroprotective and suppress damage-induced proliferation of Muller glia in the retina. Mol Cell
631 Neurosci *27*, 531–542.

632 Fischer, A.J., Foster, S., Scott, M.A., and Sherwood, P. (2008). The transient expression of LIM-
633 domain transcription factors is coincident with the delayed maturation of photoreceptors in the
634 chicken retina. J Comp Neurol *506*, 584–603.

635 Fischer, A.J., Scott, M.A., Ritchey, E.R., and Sherwood, P. (2009a). Mitogen-activated protein
636 kinase-signaling regulates the ability of Müller glia to proliferate and protect retinal neurons
637 against excitotoxicity. Glia *57*, 1538–1552.

638 Fischer, A.J., Scott, M.A., Ritchey, E.R., and Sherwood, P. (2009b). Mitogen-activated protein
639 kinase-signaling regulates the ability of Müller glia to proliferate and protect retinal neurons
640 against excitotoxicity. Glia *57*, 1538–1552.

641 Fischer, A.J., Scott, M.A., and Tuten, W. (2009c). Mitogen-activated protein kinase-signaling
642 stimulates Muller glia to proliferate in acutely damaged chicken retina. Glia *57*, 166–181.

643 Fischer, A.J., Zelinka, C., Gallina, D., Scott, M.A., and Todd, L. (2014). Reactive microglia and
644 macrophage facilitate the formation of Müller glia-derived retinal progenitors. Glia *62*, 1608–
645 1628.

646 Fischer, A.J., Zelinka, C., and Milani-Nejad, N. (2015). Reactive retinal microglia, neuronal
647 survival, and the formation of retinal folds and detachments. Glia *63*, 313–327.

648 Frampton, G., Coufal, M., Li, H., Ramirez, J., and DeMorrow, S. (2010). Opposing actions of
649 endocannabinoids on cholangiocarcinoma growth is via the differential activation of Notch
650 signaling. Exp Cell Res *316*, 1465–1478.

651 Gallina, D.Z., C.P. Cebulla, C.M. Fischer, A.J. (2015). Activation of glucocorticoid receptors in
652 Müller glia is protective to retinal neurons and suppresses microglial reactivity. Exp Neurol *273*,
653 114–125.

654 Gallina, D., Palazzo, I., Steffenson, L., Todd, L., and Fischer, A.J. (2016). Wnt/β-catenin-
655 signaling and the formation of Müller glia-derived progenitors in the chick retina. Developmental
656 Neurobiology *76*, 983–1002.

657 Ghai, K., Zelinka, C., and Fischer, A.J. (2009). Serotonin released from amacrine neurons is
658 scavenged and degraded in bipolar neurons in the retina. J Neurochem *111*, 1–14.

659 Ghai, K., Zelinka, C., and Fischer, A.J. (2010). Notch signaling influences neuroprotective and
660 proliferative properties of mature Muller glia. J Neurosci *30*, 3101–3112.

661 Hillard, C.J. (2015). The Endocannabinoid Signaling System in the CNS. In International Review
662 of Neurobiology, (Elsevier), pp. 1–47.

663 Hoang, T., Wang, J., Boyd, P., Wang, F., Santiago, C., Jiang, L., Yoo, S., Lahne, M., Todd, L.J.,
664 Jia, M., et al. (2020). Gene regulatory networks controlling vertebrate retinal regeneration.
665 Science *370*.

666 Hu, S.S.-J., Arnold, A., Hutchens, J.M., Radicke, J., Cravatt, B.F., Wager-Miller, J., Mackie, K.,
667 and Straiker, A. (2010). Architecture of cannabinoid signaling in mouse retina. J Comp Neurol
668 *518*, 3848–3866.

669 Inoue, M., Nakayama, C., and Noguchi, H. (1996). Activating mechanism of CNTF and related
670 cytokines. Mol Neurobiol *12*, 195–209.

671 Iribarne, M., Hyde, D.R., and Masai, I. (2019). TNFα Induces Müller Glia to Transition From
672 Non-proliferative Gliosis to a Regenerative Response in Mutant Zebrafish Presenting Chronic
673 Photoreceptor Degeneration. Front. Cell Dev. Biol. *7*.

674 Kokona, D., Spyridakos, D., Tzatzarakis, M., Papadogkonaki, S., Filidou, E., Arvanitidis, K.I.,
675 Kolios, G., Lamani, M., Makriyannis, A., Malamas, M.S., et al. (2021). The endocannabinoid 2-
676 arachidonoylglycerol and dual ABHD6/MAGL enzyme inhibitors display neuroprotective and
677 anti-inflammatory actions in the in vivo retinal model of AMPA excitotoxicity.
678 Neuropharmacology *185*, 108450.

679 Kridel, S.J., Axelrod, F., Rozenkrantz, N., and Smith, J.W. (2004). Orlistat Is a Novel Inhibitor of
680 Fatty Acid Synthase with Antitumor Activity. Cancer Res *64*, 2070–2075.

681 Kumar, A., and Shamsuddin, N. (2012). Retinal Muller Glia Initiate Innate Response to
682 Infectious Stimuli via Toll-Like Receptor Signaling. PLOS ONE *7*, e29830.

683 Kumar, A., Pandey, R.K., Miller, L.J., Singh, P.K., and Kanwar, M. (2013). Müller Glia in Retinal
684 Innate Immunity: A perspective on their roles in endophthalmitis. Crit Rev Immunol *33*, 119–135.

685 Liu, T., Zhang, L., Joo, D., and Sun, S.-C. (2017). NF-κB signaling in inflammation. Signal
686 Transduct Target Ther *2*, 17023.

687 Magness, S.T., Jijon, H., Van Houten Fisher, N., Sharpless, N.E., Brenner, D.A., and Jobin, C.
688 (2004). In vivo pattern of lipopolysaccharide and anti-CD3-induced NF-kappa B activation using
689 a novel gene-targeted enhanced GFP reporter gene mouse. J Immunol *173*, 1561–1570.

690 Matsuda, S., Kanemitsu, N., Nakamura, A., Mimura, Y., Ueda, N., Kurahashi, Y., and
691 Yamamoto, S. (1997). Metabolism of Anandamide, an Endogenous Cannabinoid Receptor
692 Ligand, in Porcine Ocular Tissues. Experimental Eye Research *64*, 707–711.

693 Nagarkatti, P., Pandey, R., Rieder, S.A., Hegde, V.L., and Nagarkatti, M. (2009). Cannabinoids
694 as novel anti-inflammatory drugs. Future Med Chem *1*, 1333–1349.

695 Nalli, Y., Dar, M.S., Bano, N., Rasool, J.U., Sarkar, A.R., Banday, J., Bhat, A.Q., Rafia, B.,
696 Vishwakarma, R.A., Dar, M.J., et al. (2019). Analyzing the role of cannabinoids as modulators of
697 Wnt/β-catenin signaling pathway for their use in the management of neuropathic pain.
698 Bioorganic & Medicinal Chemistry Letters *29*, 1043–1046.

699 Palazuelos, J., Ortega, Z., Díaz-Alonso, J., Guzmán, M., and Galve-Roperh, I. (2012). CB2
700 Cannabinoid Receptors Promote Neural Progenitor Cell Proliferation via mTORC1 Signaling *.
701 Journal of Biological Chemistry *287*, 1198–1209.

702 Palazzo, I., Deistler, K., Hoang, T.V., Blackshaw, S., and Fischer, A.J. (2019). NF-κB signaling
703 regulates the formation of proliferating Müller glia-derived progenitor cells in the avian retina.
704 BioRxiv 724260.

705 Palazzo, I., Deistler, K., Hoang, T.V., Blackshaw, S., and Fischer, A.J. (2020). NF-κB signaling
706 regulates the formation of proliferating Müller glia-derived progenitor cells in the avian retina.
707 Development.

708 Pertwee, R.G. (2010). Receptors and Channels Targeted by Synthetic Cannabinoid Receptor
709 Agonists and Antagonists. Curr Med Chem *17*, 1360–1381.

710 Rapino, C., Tortolani, D., Scipioni, L., and Maccarrone, M. (2018). Neuroprotection by
711 (Endo)Cannabinoids in Glaucoma and Retinal Neurodegenerative Diseases. Curr
712 Neuropharmacol *16*, 959–970.

713 Satija, R., Farrell, J.A., Gennert, D., Schier, A.F., and Regev, A. (2015). Spatial reconstruction
714 of single-cell gene expression data. Nat Biotechnol *33*, 495–502.

715 Schwitzer, T., Schwan, R., Angioi-Duprez, K., Giersch, A., and Laprevote, V. (2016). The
716 Endocannabinoid System in the Retina: From Physiology to Practical and Therapeutic
717 Applications. Neural Plast *2016*.

718 Shamsuddin, N., and Kumar, A. (2011). TLR2 mediates the innate response of retinal Muller
719 glia to Staphylococcus aureus. J Immunol *186*, 7089–7097.

720 da Silva Sampaio, L., Kubrusly, R.C.C., Colli, Y.P., Trindade, P.P., Ribeiro-Resende, V.T.,
721 Einicker-Lamas, M., Paes-de-Carvalho, R., Gardino, P.F., de Mello, F.G., and De Melo Reis,
722 R.A. (2018). Cannabinoid Receptor Type 1 Expression in the Developing Avian Retina:
723 Morphological and Functional Correlation With the Dopaminergic System. Front Cell Neurosci
724 *12*.

725 Silverman, S.M., and Wong, W.T. (2018). Microglia in the Retina: Roles in Development,
726 Maturity, and Disease. Annual Review of Vision Science *4*, 45–77.

727 Slusar, J.E., Cairns, E.A., Szczesniak, A.-M., Bradshaw, H.B., Di Polo, A., and Kelly, M.E.M.
728 (2013). The fatty acid amide hydrolase inhibitor, URB597, promotes retinal ganglion cell
729 neuroprotection in a rat model of optic nerve axotomy. Neuropharmacology *72*, 116–125.

730 Stanke, J., Moose, H.E., El-Hodiri, H.M., and Fischer, A.J. (2010). Comparative study of Pax2
731 expression in glial cells in the retina and optic nerve of birds and mammals. J Comp Neurol *518*,
732 2316–2333.

733 Stella, N. (2009). Endocannabinoid signaling in microglial cells. Neuropharmacology *56*, 244–
734 253.

735 Stincic, T.L., and Hyson, R.L. (2011). The localization and physiological effects of cannabinoid
736 receptor 1 (CB1) in the brain stem auditory system of the chick. Neuroscience *194C*, 150–159.

737 Straiker, A.J., Maguire, G., Mackie, K., and Lindsey, J. (1999). Localization of Cannabinoid CB1
738 Receptors in the Human Anterior Eye and Retina. Invest. Ophthalmol. Vis. Sci. *40*, 2442–2448.

739 Todd, L., and Fischer, A.J. (2015). Hedgehog-signaling stimulates the formation of proliferating
740 Müller glia-derived progenitor cells in the retina. Development *142*, 2610–2622.

741 Todd, L., Palazzo, I., Suarez, L., Liu, X., Volkov, L., Hoang, T.V., Campbell, W.A., Blackshaw,
742 S., Quan, N., and Fischer, A.J. (2019). Reactive microglia and IL1β/IL-1R1-signaling mediate
743 neuroprotection in excitotoxin-damaged mouse retina. Journal of Neuroinflammation *16*, 118.

744 Todd, L., Finkbeiner, C., Wong, C.K., Hooper, M.J., and Reh, T.A. (2020). Microglia Suppress
745 Ascl1-Induced Retinal Regeneration in Mice. Cell Reports *33*, 108507.

746 Ullrich, O., Merker, K., Timm, J., and Tauber, S. (2007). Immune control by endocannabinoids
747 — New mechanisms of neuroprotection? Journal of Neuroimmunology *184*, 127–135.

748 White, D.T., Sengupta, S., Saxena, M.T., Xu, Q., Hanes, J., Ding, D., Ji, H., and Mumm, J.S.
749 (2017). Immunomodulation-accelerated neuronal regeneration following selective rod
750 photoreceptor cell ablation in the zebrafish retina. PNAS *114*, E3719–E3728.

751 Xu, J.-Y., and Chen, C. (2015). Endocannabinoids in Synaptic Plasticity and Neuroprotection.
752 Neuroscientist *21*, 152–168.

753 Yang, W., Li, Q., Wang, S.-Y., Gao, F., Qian, W.-J., Li, F., Ji, M., Sun, X.-H., Miao, Y., and
754 Wang, Z. (2016). Cannabinoid receptor agonists modulate calcium channels in rat retinal müller
755 cells. Neuroscience *313*, 213–224.

756 Yazulla, S., Studholme, K.M., McINTOSH, H.H., and Fan, S.-F. (2000). Cannabinoid receptors
757 on goldfish retinal bipolar cells: Electron-microscope immunocytochemistry and whole-cell
758 recordings. Visual Neuroscience *17*, 391–401.

759 Zelinka, C.P., Volkov, L., Goodman, Z.A., Todd, L., Palazzo, I., Bishop, W.A., and Fischer, A.J.
760 (2016). mTor signaling is required for the formation of proliferating Müller glia-derived progenitor
761 cells in the chick retina. Development *143*, 1859–1873.

762 Zhao, X.F., Wan, J., Powell, C., Ramachandran, R., Myers, M.G., Jr., and Goldman, D. (2014).
763 Leptin and IL-6 family cytokines synergize to stimulate muller glia reprogramming and retina
764 regeneration. Cell Rep *9*, 272–284.

765
766

Figure legends:

Figure 1. eCB-related genes are widely expressed in different types of retinal cells. Panel **a** illustrates a schematic diagram of the enzymes and receptors involved in eCB synthesis, degradation and signaling. scRNA-seq was used to identify patterns of expression of eCB-related genes among retinal cells. Patterns and levels of expression are presented in UMAP plots (**b**-**h**) and violin plots (**i**). scRNA-seq libraries were aggregated from control and treated 3hr, 12hr, and 48hr after NMDA-treatment (**b**). UMAP-ordered cells formed distinct clusters of neuronal cells, resting MG, early activated MG, activated MG and late activated MG (**c-e**). UMAP heatmaps of *CNR1*, *MGLL, NAPEPLD, DAGLA, DAGLB* and *FAAH* demonstrate patterns and levels of expression across different retinal cells, with black dots representing cells with expression of 2 or more genes (**f**-**h**). Violin plots illustrate relative levels and percent of expression in resting and activated MG (**i**). Violin plots illustrate levels of gene expression and significant changes (*p<0.01, **p<10exp-10, ***p<10exp-20) in levels that were determined by using a Wilcox rank sum with Bonferroni correction.

Figure 2. eCB-related genes are dynamically expressed by MG in response to damage or growth-factor treatment. scRNA-seq was used to identify patterns of expression of eCB genes in MG at several time points after NMDA damage or FGF + insulin growth factor treatment to form MGPCs. UMAP- clusters of MG were identified by expression of hallmark genes (**a,b,d**). Progenitors were then classified by different cell cycle and progenitor markers (**c, e, f**). Each dot represents one cell and black dots

indicate cells with 2 or more genes expressed. The expression of eCB related genes was illustrated in a colored heatmap and in a violin plot violin plot with population percentages and statistical comparisons. (**g,h,i**). Significant difference (*p<0.01, **p<0.0001, ***p<<0.0001) was determined by using a Wilcox rank sum with Bonferroni correction. MG – Müller glia, MGPC – Müller glia-derived progenitor cell.

Figure 3. eCB increase numbers of proliferating MGPCs in damaged retinas. Chick eyes were injected with NMDA, AEA, 2-AG, and EdU according to the paradigm at the top figure. Eyes were harvested at 24 hrs after the last injection and retinas processed for immunolabeling. Retinas were labeled for Sox2 (green) and EdU^+ (red) cells (**a**), neurofilament (red), phospho-Histone H3 (pHisH3, green), and DAPI (blue; **d**). Dying cells were labeled using the TUNEL assay (**e**). Histograms illustrate the mean (± SD) and each dot represents one biological replicate. Significance of difference (**p<0.01, ***p<0.001) was determined by using a paired *t*-test. Arrows indicate the nuclei of MG. The calibration bar panels **a, d** and **e** represent 50 µm. Abbreviations: ONL – outer nuclear layer, INL – inner nuclear layer, IPL – inner plexiform layer, GCL – ganglion cell layer, NF – neurofilament, ns – not significant.

Figure 4. Small molecule drug targeting CNR1, DAGL and MGLL influence the formation of MGPCs. The treatment paradigm is illustrated at the top of the figure. Compounds included Orlistat (DAGL inhibitor), JJKK048 (MGLL inhibitor), Win55 (CNR1 agonist), and Rimonabant (CNR1 antagonist). Competitive inhibitor ELISAs of illustrate relative levels of 2-AG and AEA after NMDA damage and treatment with Orlistat or JJKK048 (**a,b**). Retinas were labeled for Sox2 (green) and EdU (red; **a**).

Arrows indicate EdU+/Sox2+ nuclei of MGPCs, small double-arrows indicate EdU+/Sox2+ nuclei of NIRG cells in the IPL, and hollow arrow-heads indicate EdU+/Sox- nuclei of presumptive microglia. The histograms in **a,b** and **d-g** represents the mean (± SD) and each dot represents one biological replicate retina. The calibration bar in **c** represents 50 µm. Abbreviations: ONL – outer nuclear layer, INL – inner nuclear layer, IPL – inner plexiform layer, GCL – ganglion cell layer.

Figure 5. Targeting the AEA pathway does not influence the formation of MGPCs. The treatment paradigm is illustrated at the top of the figure. Compounds included ARN19874 (NAPEPLD inhibitor), URB597 (FAAH inhibitor) and PF-044 (FAAH inhibitor). Eyes were harvested at 24 hrs after the last injection and retinas processed for immunofluorescence. Retinal sections were labeled for Sox2 (green) and EdU (red; **a**), CD45 (green) and EdU (red; **c**), Nkx2.2 (green) and EdU (red, **e**), and cell death (TUNEL, red; **g**). The histograms in **b,d**,**f,h** represents the mean (± SD) number of proliferating MGPCs (**b**), proliferating microglia (**d**), proliferating NIRG cells (**f**), and dying cells (**h**). Each dot represents one biological replicate retina. Arrows indicate EdU+/Sox2+ nuclei of MGPCs, small double-arrows indicate EdU+/Nkx2.2+ nuclei of NIRG cells in the IPL, and hollow arrow-heads indicate EdU+/CD45+ nuclei of microglia. The calibration bar in **g** represents 50 µm and applies to panels **a,c,e** and **g**. Abbreviations: ONL – outer nuclear layer, INL – inner nuclear layer, IPL – inner plexiform layer, GCL – ganglion cell layer. Microglia were from aggregate scRNA-seq libraries were re-embedded and ordered in UMAP (**i**). Microglia from saline- and NMDA-treated retinas were clustered into resting, active and early activated cells (**j**). Clusters

838 of cells were arranged according to markers such as *TNFSF15, PPARG, IL1R2, DBI*
839 and *AIR1L* (**k,l**). *MGLL* and *NAPEPLD* had scattered expression across microglia in
840 different clusters, whereas *CNR1* was not widely expressed (**m**).
841
842 **Figure 6. Microglia reactivity in damaged retina treated with eCBs.** The treatment
843 paradigm is illustrated at the top of the figure. Compounds included 2-AG+AEA (CNR1
844 agonists), Orlistat (DAGL inhibitor), JJKK048 (MGLL inhibitor), Win55 (CNR1 agonist),
845 and Rimonabant (CNR1 antagonist). Eyes were harvested 24hrs after the last injection
846 and retinas were processed for immunofluorescence. Retinal sections were labeled for
847 CD45 (green) and DAPI (blue; **a**), or CD45 (green), EdU (red) and DAPI (blue; **b**).
848 Microglial reactivity was assessed by measuring CD45 area and intensity, proliferation
849 (EdU+), and total number of microglia (CD45+/DRAQ5+) (**b**). Arrows indicate the nuclei
850 of microglia. Histograms in **c** illustrate the mean (±SD, control n = 40, treatment n = 8)
851 and each symbol represents one biological replicate. The shape of the microglia was
852 assessed using a Sholl analysis. Representative microglia from each condition is
853 shown, with a heat map of radial intersections (blue = low, red/white = high) (**c**). The
854 graph in **d** illustrates of the number of processes radially (µm±SE) from microglial nuclei
855 from control (n=15) and NMDA damaged (n = 25) retinas. (**d**) Significance of difference
856 was determined by using a one way ANOVA with corresponding Tukey's test. The
857 calibration bars panels **a, b** represent 50 µm, and the bar in d represents 5 µM**.**
858 Abbreviations: ONL – outer nuclear layer, INL – inner nuclear layer, IPL – inner
859 plexiform layer, GCL – ganglion cell layer.
860

Figure 7. Patterns of expression of eCB-related genes in normal and NMDA-damaged mouse retinas. Cells were obtained from control retinas and from retinas at 3, 6, 12, 24, 36, 48 and 72hrs after NMDA-treatment and clustered in UMAP plots with each dot representing an individual cell (**a**). UMAP plots revealed distinct clustering of different types of retinal cells; resting MG (a mix of control, 48hr and 72hr NMDA-tr), 12-72 hr NMDA-tr MG (activated MG in violin plots), 6hrs NMDA-tr MG, 3hrs NMDA-tr MG, microglia, astrocytes, RPE cells, endothelial cells, retinal ganglion cells, horizontal cells (HCs), amacrine cells (ACs), bipolar cells (BPs), rod photoreceptors, and cone photoreceptors (**b**). Resting and activated MG were identified based on patterns of expression of *Slc1a3, Nes* and *Vim* (**c**). Cells were colored with a heatmap of expression of Cnr1*, Daglb, Mgll, Napepld and Faah* expression (**d**-**f**). Black dots indicate cells that express two or more markers.

Figure 8. eCBs and NF-kB-signaling in MG of damaged mouse retinas

The treatment paradigm is illustrated at the top of the figure. Eyes of mice (cis-NF-kB^{eGFP}) were pretreated with compounds or vehicle prior to NMDA + vehicle/compound, and retinas harvested 24 hrs after the last injection. Compounds included 2-AG+AEA (CNR1 agonists), Win55 (CNR1 agonist), and Rimonabant (CNR1 antagonist). Retinal sections were labeled for Sox9 (blue) and eGFP (green) (**b**), fragmented DNA using the TUNEL method (**d**), and Iba1 (red) and Draq5 (blue; **f**). The histogram/scatter-plots illustrate the mean (±SD) number of eGFP+ MG (**c**), dying cells (**e**) or Iba1+/Draq5+ cells (**g**). Each dot represents one biological replicate. Significance of difference (*p<0.05) was determined by using a paired *t*-test. The calibration bars panels **a**, **c, e,**

884 and **g** represent 50 µm. Abbreviations: ONL – outer nuclear layer, INL – inner nuclear
885 layer, IPL – inner plexiform layer, GCL – ganglion cell layer.
886
887 **Figure 9. Summary Schematic of eCB effect on MG reprogramming.** Using scRNA-
888 seq analysis, we identified patterns of expression of genes involved in eCB synthesis,
889 degradation and signaling (**a**). ELISAs indicated a more prominent role of 2-AG over
890 AEA, and drugs which elevated 2-AG signaling increased MGPCs after damage (**b**).
891 Microglia were unresponsive to these treatments and retained a reactive phenotype in a
892 damaged retina (**c**). In the NF-kBeGFP+ reporter mice, damage activates signaling in
893 MG, which is decreased by exogenous eCBs or CNR1 agonists (**d**).
894
895 **Table 1**. **Sholl Analysis of microglia from the chick retina after damage and eCB**
896 **treatment.** Statistical analysis was performed with a one-way ANOVA and Tukey's test
897 (NMDA n = 25, treatments n = 15)
898

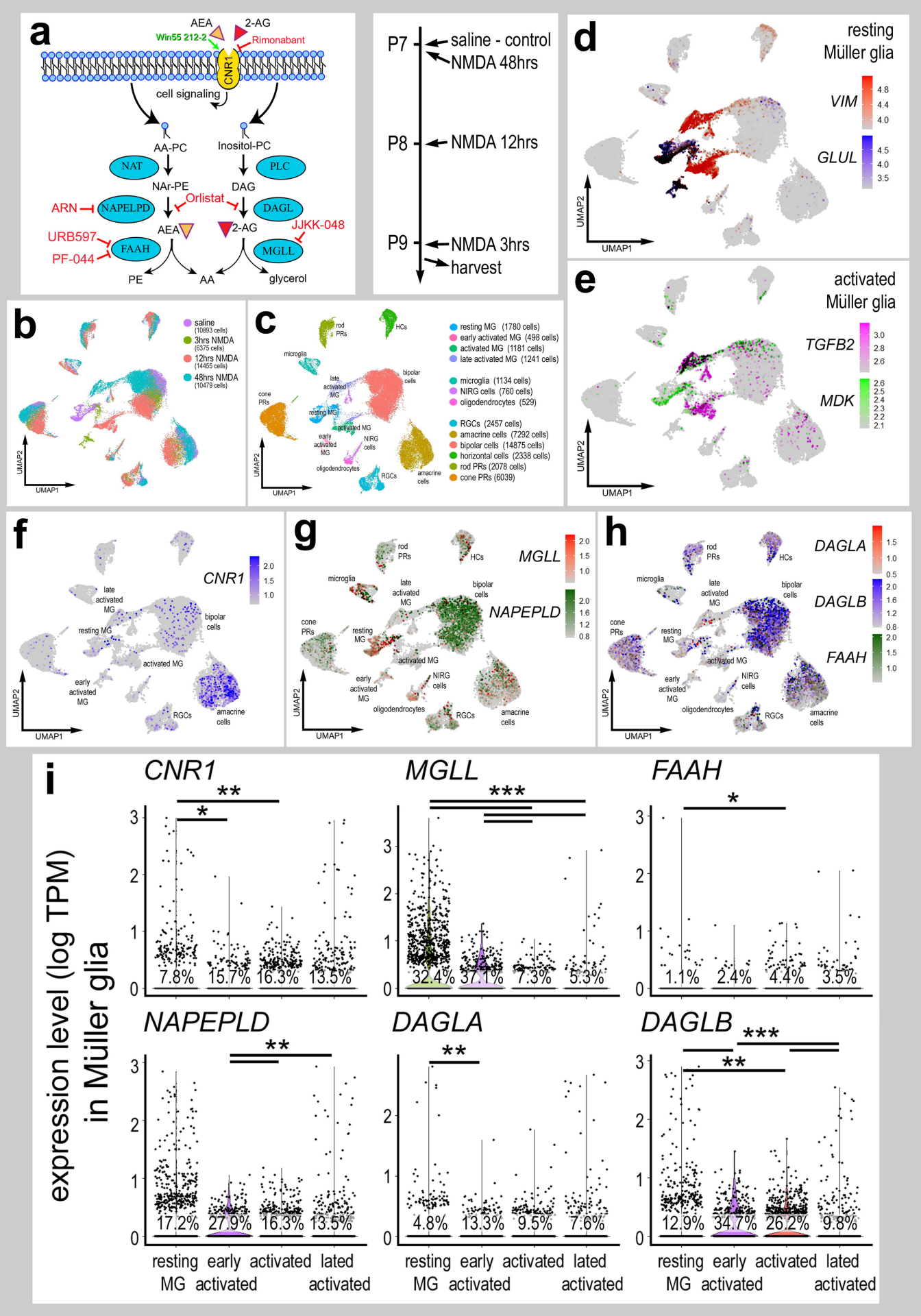
a
AEA
2-AG
Win55 212-2
Rimonabant
CNR1
cell signaling
AA-PC
Inositol-PC
NAT
PLC
NAr-PE
DAG
ARN
NAPELPD
Orlistat
DAGL
AEA
2-AG
JJKK-048
URB597
FAAH
PF-044
MGLL
PE
AA
glycerol
P7
saline - control
NMDA 48hrs
P8
NMDA 12hrs
P9
NMDA 3hrs
harvest
b
saline (10893 cells)
3hrs NMDA (6375 cells)
12hrs NMDA (14455 cells)
48hrs NMDA (10479 cells)
UMAP2
UMAP1
c
rod PRs
HCs
microglia
late activated MG
bipolar cells
cone PRs
resting MG
activated MG
early activated MG
NIRG cells
oligodendrocytes
RGCs
amacrine cells
resting MG (1780 cells)
early activated MG (498 cells)
activated MG (1181 cells)
late activated MG (1241 cells)
microglia (1134 cells)
NIRG cells (760 cells)
oligodendrocytes (529)
RGCs (2457 cells)
amacrine cells (7292 cells)
bipolar cells (14875 cells)
horizontal cells (2338 cells)
rod PRs (2078 cells)
cone PRs (6039)
d
resting Müller glia
VIM
GLUL
e
activated Müller glia
TGFB2
MDK
f
CNR1
g
MGLL
NAPEPLD
h
DAGLA
DAGLB
FAAH
i
expression level (log TPM) in Müller glia
CNR1
MGLL
FAAH
NAPEPLD
DAGLA
DAGLB
7.8%
15.7%
16.3%
13.5%
32.4%
37.1%
7.3%
5.3%
1.1%
2.4%
4.4%
3.5%
17.2%
27.9%
16.3%
13.5%
4.8%
13.3%
9.5%
7.6%
12.9%
34.7%
26.2%
9.8%
resting MG
early activated
activated
lated activated

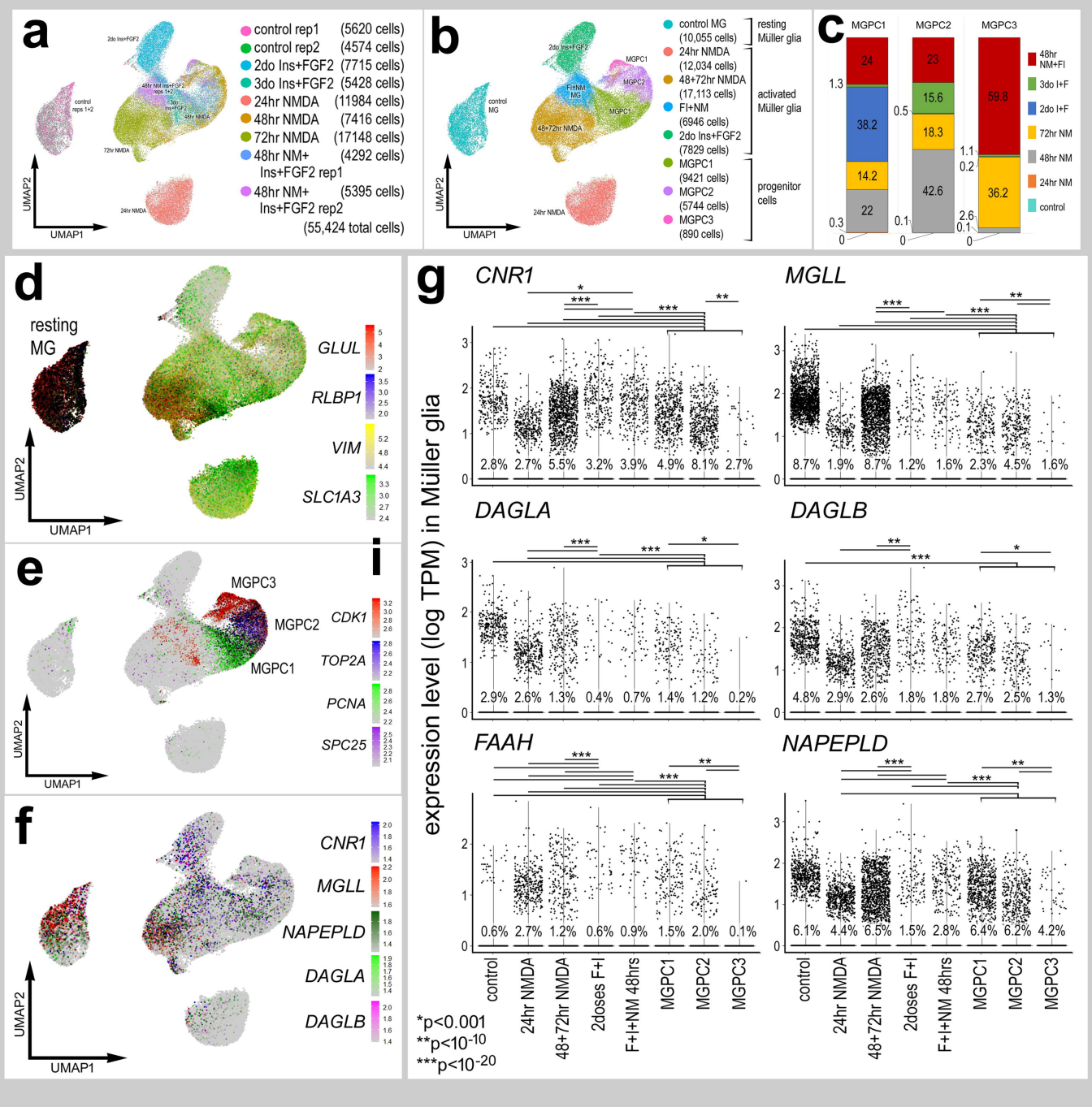
a
control rep1 (5620 cells)
control rep2 (4574 cells)
2do Ins+FGF2 (7715 cells)
3do Ins+FGF2 (5428 cells)
24hr NMDA (11984 cells)
48hr NMDA (7416 cells)
72hr NMDA (17148 cells)
48hr NM+ Ins+FGF2 rep1 (4292 cells)
48hr NM+ Ins+FGF2 rep2 (5395 cells)
(55,424 total cells)
b
control MG (10,055 cells)
24hr NMDA (12,034 cells)
48+72hr NMDA (17,113 cells)
FI+NM (6946 cells)
2do Ins+FGF2 (7829 cells)
MGPC1 (9421 cells)
MGPC2 (5744 cells)
MGPC3 (890 cells)
resting Müller glia
activated Müller glia
progenitor cells
c
MGPC1
MGPC2
MGPC3
48hr NM+FI
3do I+F
2do I+F
72hr NM
48hr NM
24hr NM
control
d
resting MG
GLUL
RLBP1
VIM
SLC1A3
e
MGPC3
MGPC2
MGPC1
i
CDK1
TOP2A
PCNA
SPC25
f
CNR1
MGLL
NAPEPLD
DAGLA
DAGLB
UMAP1
UMAP2
g
CNR1
MGLL
DAGLA
DAGLB
FAAH
NAPEPLD
expression level (log TPM) in Müller glia
control
24hr NMDA
48+72hr NMDA
2doses F+I
F+I+NM 48hrs
MGPC1
MGPC2
MGPC3
*p<0.001
**p<10-10
***p<10-20

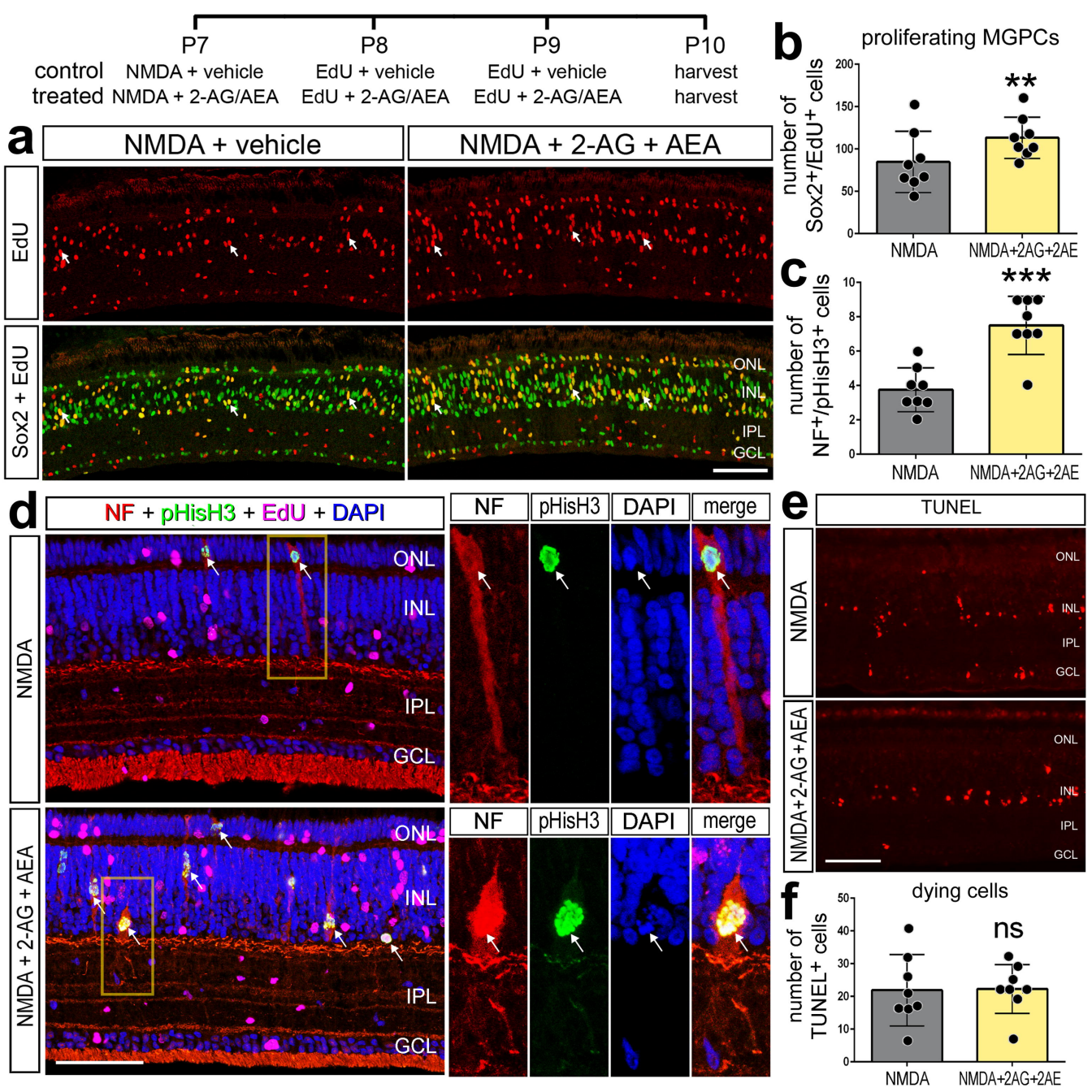
P7
P8
P9
P10
control
treated
NMDA + vehicle
NMDA + 2-AG/AEA
EdU + vehicle
EdU + 2-AG/AEA
EdU + vehicle
EdU + 2-AG/AEA
harvest
harvest
a
NMDA + vehicle
NMDA + 2-AG + AEA
EdU
Sox2 + EdU
ONL
INL
IPL
GCL
b
proliferating MGPCs
number of Sox2+/EdU+ cells
**
NMDA
NMDA+2AG+2AE
c
number of NF+/pHisH3+ cells
***
NMDA
NMDA+2AG+2AE
d
NF + pHisH3 + EdU + DAPI
NMDA
NMDA + 2-AG + AEA
ONL
INL
IPL
GCL
NF
pHisH3
DAPI
merge
e
TUNEL
NMDA
NMDA+2-AG+AEA
f
dying cells
number of TUNEL+ cells
ns
NMDA
NMDA+2AG+2AE

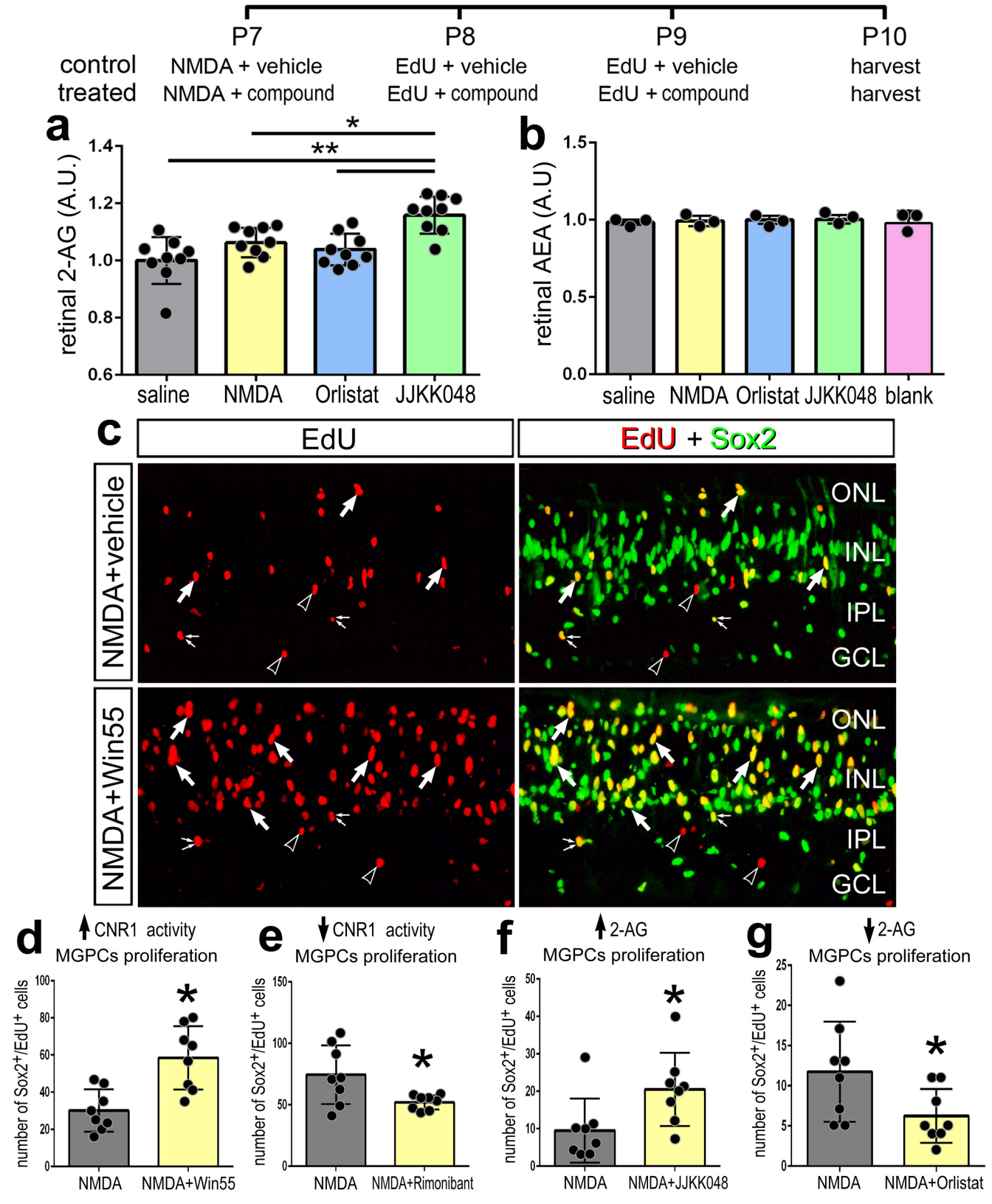
P7
P8
P9
P10
control
treated
NMDA + vehicle
NMDA + compound
EdU + vehicle
EdU + compound
EdU + vehicle
EdU + compound
harvest
harvest
a
retinal 2-AG (A.U.)
saline
NMDA
Orlistat
JJKK048
b
retinal AEA (A.U)
saline
NMDA
Orlistat
JJKK048
blank
c
EdU
EdU + Sox2
NMDA+vehicle
NMDA+Win55
ONL
INL
IPL
GCL
d
CNR1 activity
MGPCs proliferation
number of Sox2+/EdU+ cells
NMDA
NMDA+Win55
e
CNR1 activity
MGPCs proliferation
number of Sox2+/EdU+ cells
NMDA
NMDA+Rimonibant
f
2-AG
MGPCs proliferation
number of Sox2+/EdU+ cells
NMDA
NMDA+JJKK048
g
2-AG
MGPCs proliferation
number of Sox2+/EdU+ cells
NMDA
NMDA+Orlistat

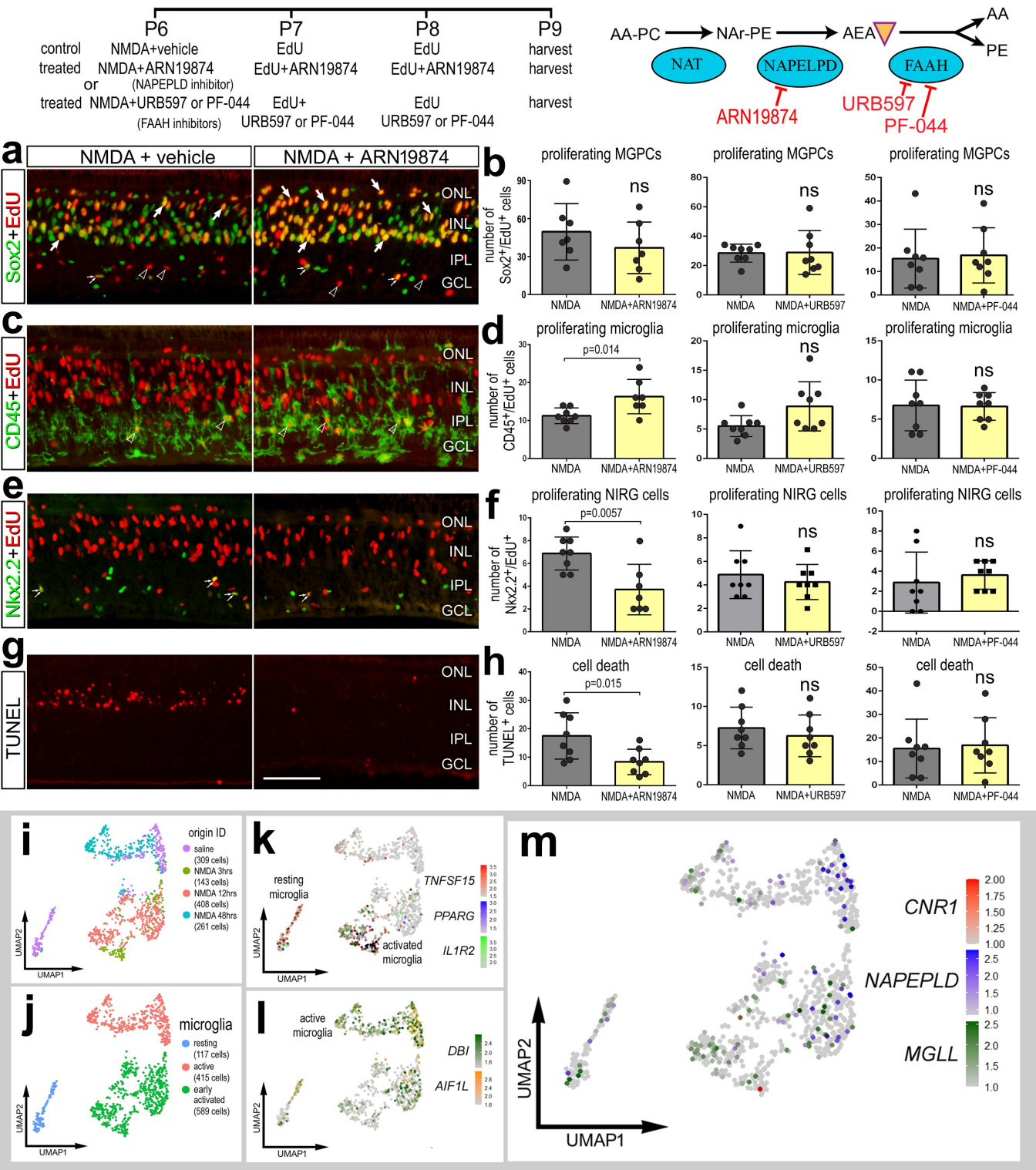
P6
P7
P8
P9
control treated
NMDA+vehicle
EdU
EdU
harvest
or
NMDA+ARN19874
(NAPEPLD inhibitor)
EdU+ARN19874
EdU+ARN19874
harvest
treated
NMDA+URB597 or PF-044
(FAAH inhibitors)
EdU+
URB597 or PF-044
EdU
URB597 or PF-044
harvest
AA-PC
NAr-PE
AEA
AA
PE
NAT
NAPELPD
FAAH
ARN19874
URB597
PF-044
a
NMDA + vehicle
NMDA + ARN19874
Sox2+EdU
CD45+EdU
Nkx2.2+EdU
TUNEL
ONL
INL
IPL
GCL
b
proliferating MGPCs
number of Sox2+/EdU+ cells
ns
NMDA
NMDA+ARN19874
NMDA+URB597
NMDA+PF-044
c
d
proliferating microglia
number of CD45+/EdU+ cells
p=0.014
e
f
proliferating NIRG cells
number of Nkx2.2+/EdU+
p=0.0057
g
h
cell death
number of TUNEL+ cells
p=0.015
i
origin ID
saline (309 cells)
NMDA 3hrs (143 cells)
NMDA 12hrs (408 cells)
NMDA 48hrs (261 cells)
UMAP1
UMAP2
j
microglia
resting (117 cells)
active (415 cells)
early activated (589 cells)
k
resting microglia
activated microglia
TNFSF15
PPARG
IL1R2
l
active microglia
DBI
AIF1L
m
CNR1
NAPEPLD
MGLL

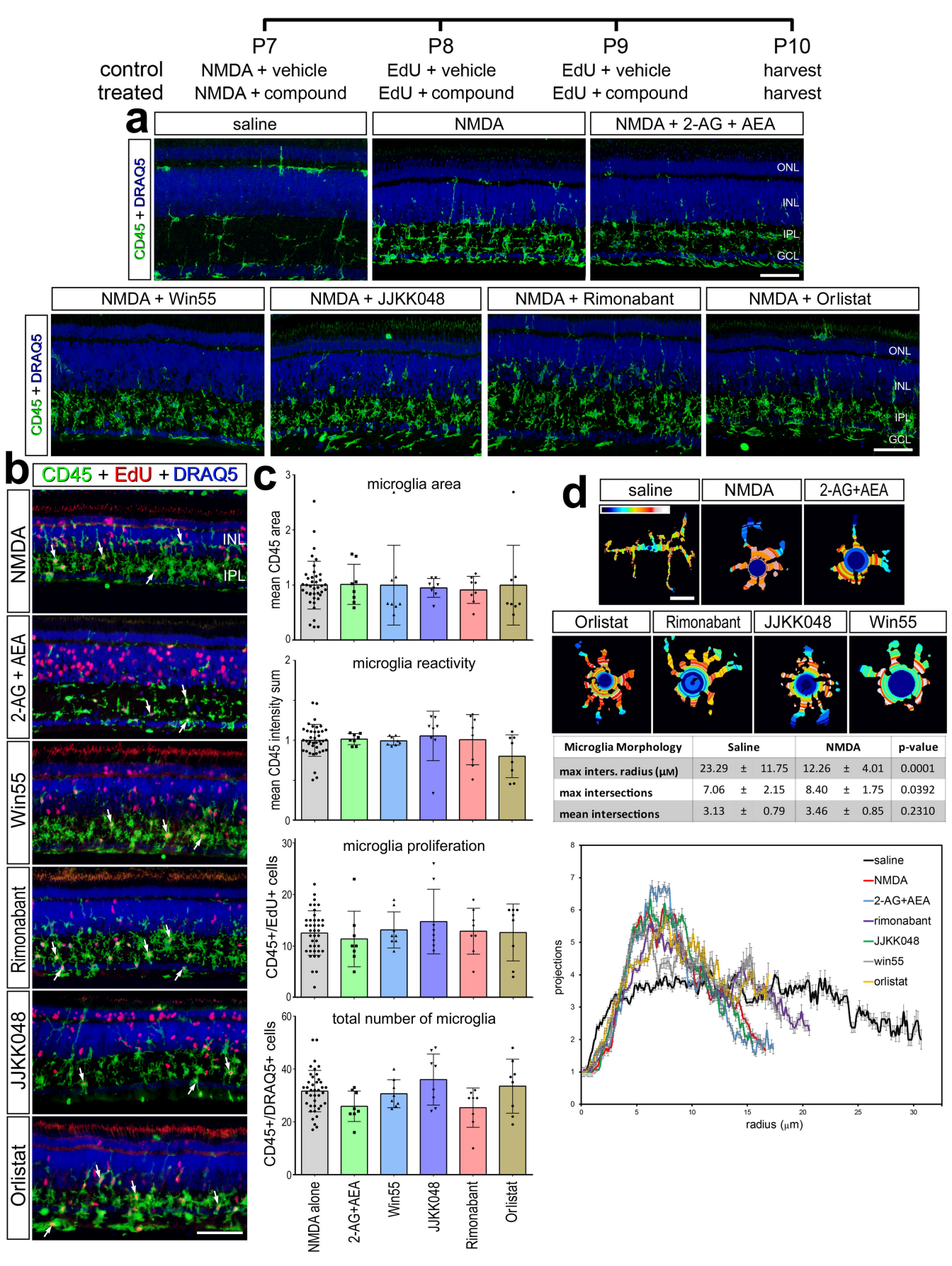

Microglia Morphology	Saline	NMDA	p-value
max inters. radius (μm)	23.29 ± 11.75	12.26 ± 4.01	0.0001
max intersections	7.06 ± 2.15	8.40 ± 1.75	0.0392
mean intersections	3.13 ± 0.79	3.46 ± 0.85	0.2310

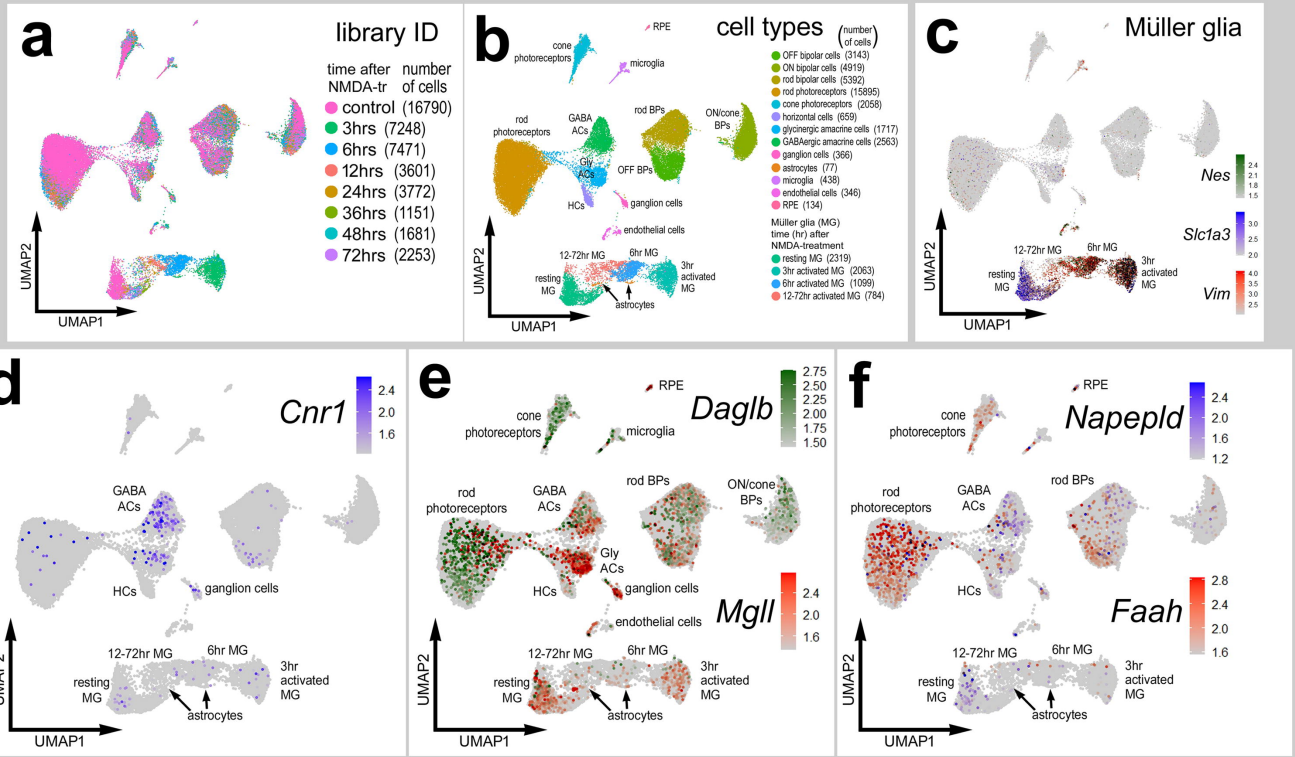
a
library ID
time after NMDA-tr
number of cells
control (16790)
3hrs (7248)
6hrs (7471)
12hrs (3601)
24hrs (3772)
36hrs (1151)
48hrs (1681)
72hrs (2253)
UMAP2
UMAP1
b
cell types
(number of cells)
RPE
cone photoreceptors
microglia
rod photoreceptors
GABA ACs
rod BPs
ON/cone BPs
Gly ACs
OFF BPs
HCs
ganglion cells
endothelial cells
12-72hr MG
6hr MG
3hr activated MG
resting MG
astrocytes
OFF bipolar cells (3143)
ON bipolar cells (4919)
rod bipolar cells (5392)
rod photoreceptors (15895)
cone photoreceptors (2058)
horizontal cells (659)
glycinergic amacrine cells (1717)
GABAergic amacrine cells (2563)
ganglion cells (366)
astrocytes (77)
microglia (438)
endothelial cells (346)
RPE (134)
Müller glia (MG) time (hr) after NMDA-treatment
resting MG (2319)
3hr activated MG (2063)
6hr activated MG (1099)
12-72hr activated MG (784)
c
Müller glia
Nes
Slc1a3
Vim
d
Cnr1
e
Daglb
Mgll
f
Napepld
Faah

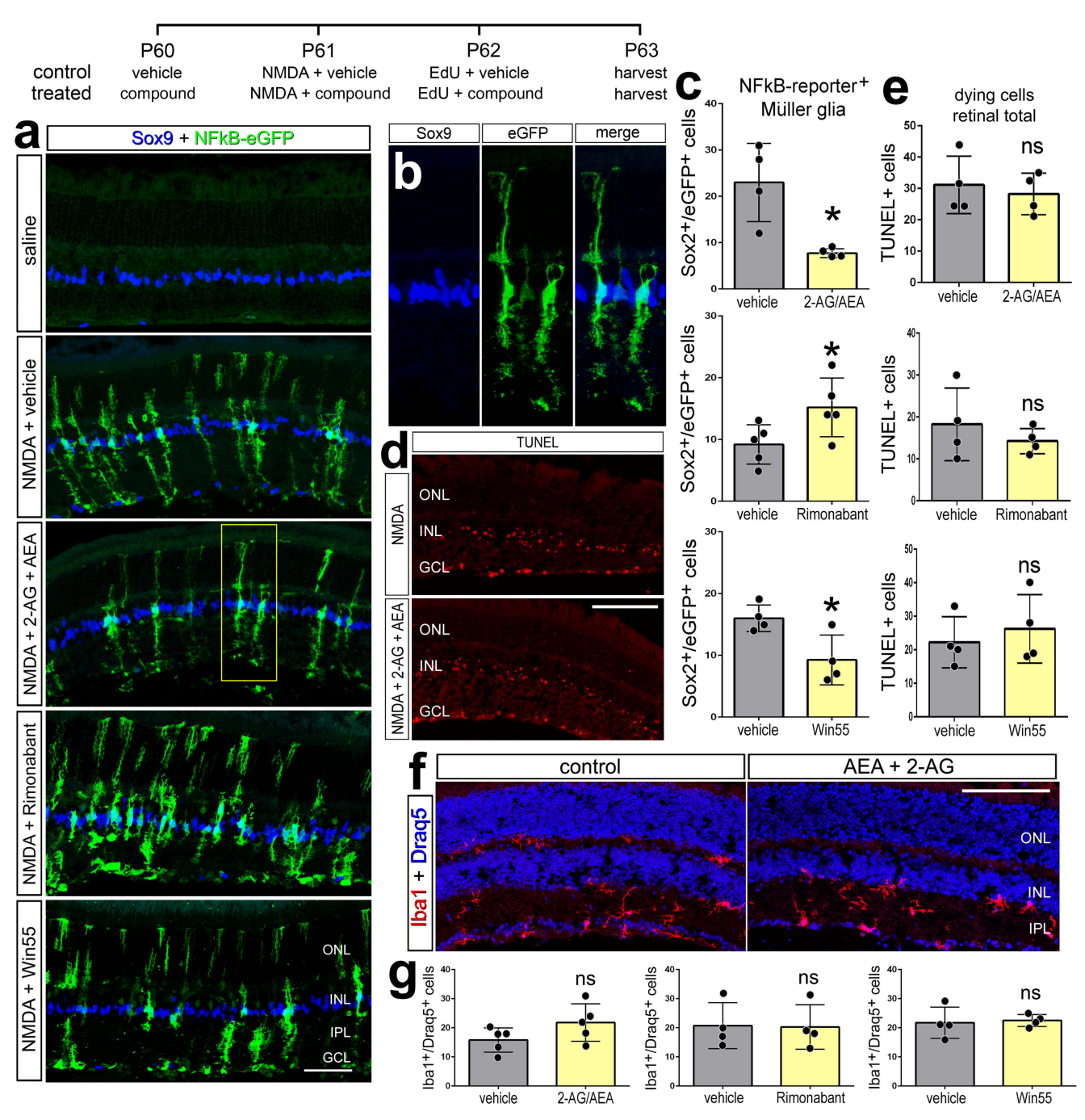
P60
vehicle
compound
P61
NMDA + vehicle
NMDA + compound
P62
EdU + vehicle
EdU + compound
P63
harvest
harvest
control
treated
a
Sox9 + NFkB-eGFP
saline
NMDA + vehicle
NMDA + 2-AG + AEA
NMDA + Rimonabant
NMDA + Win55
ONL
INL
IPL
GCL
b
Sox9
eGFP
merge
c
NFkB-reporter+
Müller glia
Sox2+/eGFP+ cells
vehicle
2-AG/AEA
Rimonabant
Win55
d
TUNEL
NMDA
NMDA + 2-AG + AEA
ONL
INL
GCL
e
dying cells
retinal total
TUNEL+ cells
ns
f
control
AEA + 2-AG
Iba1 + Draq5
ONL
INL
IPL
g
Iba1+/Draq5+ cells
vehicle
2-AG/AEA
Rimonabant
Win55
ns

A

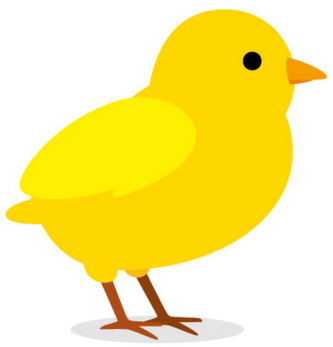

scRNA-seq

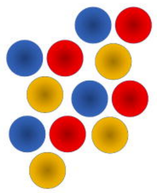

2-AG ELISA

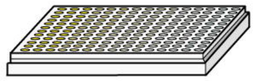

DAGB

MG

MGLL

MG

CNR1

MG

NMDA

0 4 12 24 48 72 (hrs)

JJKK048

2-AG

retina

AEA

retina

B

2-AG signaling

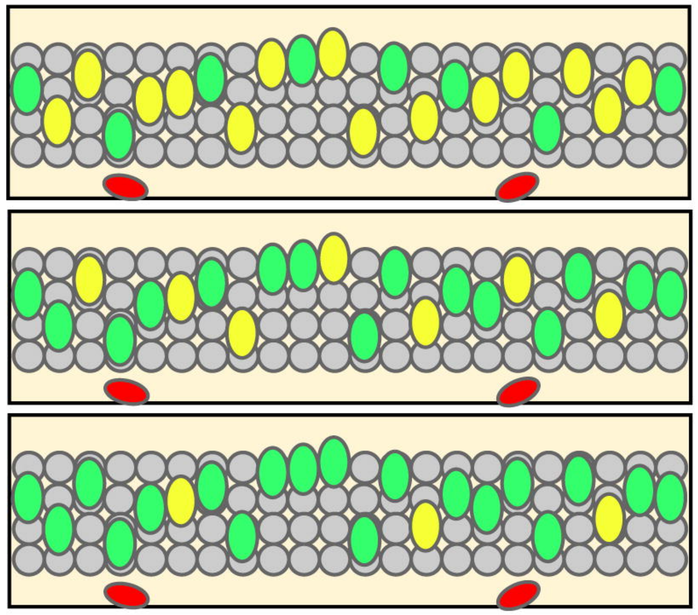

Sox2⁺ EdU⁺ MGPCs

C

NMDA

Saline NMDA NMDA + eCBs

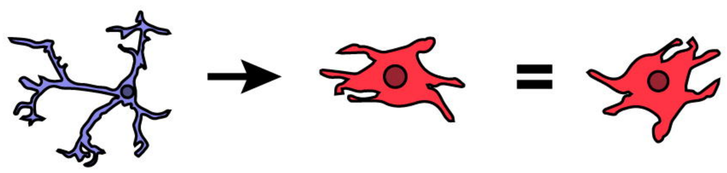

quiescent reactive reactive

cis-NF-κB^{EGFP}

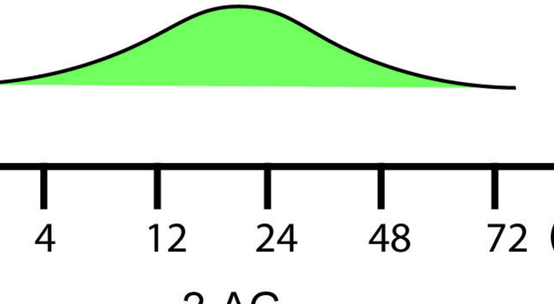

D

saline

NMDA

CNR1 agonist

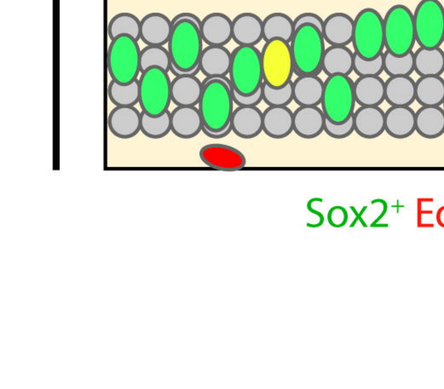

CNR1 antagonist

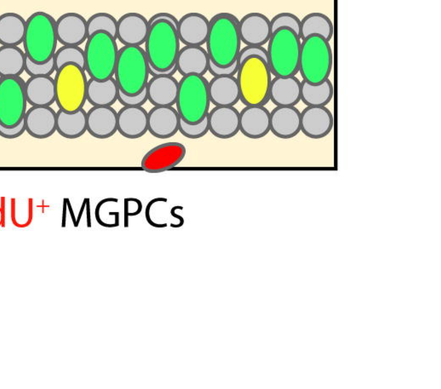

ONL

INL

IPL

GCL

	vehicle	enhance signal			dampen signal		ANOVA
Microglia Morphology	NMDA	2AG + AEA	JJKK-048	Win55-212,2	Rimonabant	Orlistat	p-value
max inters. radius (μM)	12.26 ± 4.01	11.90 ± 3.72	11.99 ± 3.51	12.65 ± 5.44	14.01 ± 5.83	12.27 ± 2.96	0.782
mean intersections	8.40 ± 1.75	7.93 ± 1.83	8.80 ± 2.54	7.40 ± 1.76	8.20 ± 1.85	9.13 ± 1.88	0.189
max intersections	3.46 ± 0.85	3.36 ± 0.61	3.58 ± 0.86	3.44 ± 0.81	3.63 ± 0.70	0.36 ± 0.68	0.921